SEC is an anti-angiogenic virulence factor that promotes *Staphylococcus aureus* Infective Endocarditis Independent of Superantigen Activity

Kyle J. Kinney[1], Sharon S. Tang[2], Xiao-Jun Wu[2], Phuong M. Tran[1, 2], Nikhila S. Bharadwaj[3], Katherine N. Gibson-Corley[4], Ana N. Forsythe[1], Katarina Kulhankova[5], Jenny E. Gumperz[3], and Wilmara Salgado-Pabón[2*]

[1]Department of Microbiology and Immunology, University of Iowa, Iowa City, Iowa, USA. [2]Department of Pathobiological Sciences, University of Wisconsin-Madison, Madison, Wisconsin, USA. [3]Department of Medical Microbiology and Immunology, University of Wisconsin-Madison, Madison, Wisconsin, USA. [4]Department of Pathology, Microbiology and Immunology, Vanderbilt University Medical Center, Nashville, Tennessee, USA. [5]Department of Pediatrics, University of Iowa, Iowa City, Iowa, USA. *corresponding author: wsalgado@wisc.edu

Abstract

The superantigen staphylococcal enterotoxin C (SEC) is critical for *Staphylococcus aureus* infective endocarditis (SAIE) in rabbits. Superantigenicity, its hallmark function, was proposed to be a major underlying mechanism driving SAIE but was not directly tested. With the use of *S. aureus* MW2 expressing SEC toxoids, we show that superantigenicity does not sufficiently account for vegetation growth, myocardial inflammation, and acute kidney injury in the rabbit model of native valve SAIE. These results highlight the critical contribution of an alternative function of superantigens to SAIE. In support of this, we provide evidence that SEC exerts anti-angiogenic effects by inhibiting branching microvessel formation in an *ex vivo* rabbit aortic ring model and by inhibiting endothelial cell expression of one of the most potent mediators of angiogenesis, VEGF-A. SEC's ability to interfere with tissue re-

25 vascularization and remodeling after injury serves as a mechanism to promote SAIE and its life-
26 threatening systemic pathologies.
27
28 **Introduction**
29 *Staphylococcus aureus* is the leading cause of infective endocarditis (IE) in high-income
30 countries *(1–3)*. *S. aureus* IE (SAIE) is an acute and invasive infection of the cardiac endothelium
31 characterized by the appearance of vegetative lesions that form predominantly on heart valves *(4)*. The
32 pathognomonic vegetations are a meshwork of bacterial aggregates and host factors such as fibrin,
33 fibrinogen, platelets, and erythrocytes that form predominantly on heart valves *(5)*. SAIE results in
34 significant damage to cardiac structures, in particular the valves and myocardium, due to tissue toxicity
35 and necropurulent inflammation *(6)*. Once established, SAIE can lead to severe complications, most
36 notably congestive heart failure, stroke, acute kidney injury, and septic shock *(3, 6, 7)*. Treatment of
37 SAIE is challenging, requiring prolonged antibiotic therapy or surgery to remove infected valves *(3, 6)*.
38 Even with treatment, SAIE has a high rate of recurrence and a 22-66% mortality rate *(1, 3)*. Infections
39 are frequently associated with methicillin-resistant *S. aureus* (MRSA) which complicate treatment and
40 increase risk of mortality *(8)*. Furthermore, life-saving medical interventions (e.g., valve replacement,
41 cardiac devices, and hemodialysis), an increasing population with underlying conditions (e.g., diabetes
42 mellitus and immunosuppression), and advanced age also increase the risk of acquiring SAIE *(1, 3)*. As
43 a result, the incidence of SAIE has continued to increase *(3)*. Unfortunately, the advances in
44 cardiovascular medicine achieved in the last decade have failed to improve SAIE outcomes. Thus,
45 understanding the mechanisms driving SAIE pathophysiology is not only of fundamental interest,
46 particularly as it relates to bacterial factors critical for vegetation formation and secondary
47 complications, but also of utmost importance to develop effective intervention strategies.
48 Epidemiological studies demonstrate a strong association between SAIE and a select group of
49 superantigen (SAg) genes, where 18-25% of SAIE clinical isolates encode *entC* (staphylococcal
50 enterotoxin C; SEC), 9-20% encode *tstH* (toxic shock syndrome toxin; TSST1), and 58-90% encode the

51 enterotoxin gene cluster (*egc*) *(9)*. Consistent with these studies, SEC, TSST1, and the *egc* SAgs SEI,
52 SEM, SEO, and SE *like* (*l*)-U all contribute to IE and metastatic infection in experimental IE *(10, 11)*.
53 However, the underlying mechanism by which SAgs contribute to SAIE pathogenesis remains
54 speculative. Classically, SAgs are known for their potent T cell mitogenic activity resulting in
55 dysregulated activation and cytokine production leading to inflammatory syndromes, and in extreme
56 cases, toxic shock *(12)*. Superantigenicity results from toxin cross-linking of the Vβ chain of the T-cell
57 receptor (TCR) to the major histocompatibility complex class II (MHC-II) receptor on antigen
58 presenting cells *(12)*. Of relevance to SAIE, endothelial cells also express MHC-II and function as
59 conditional antigen presenting cells capable of cross-linking Vβ–TCR resulting in endothelium-
60 mediated superantigenicity *(13)*.
61 The dysregulated immune activation caused by SAgs distracts and diverts the immune system
62 *(14)*. It is also the etiology of multiple diseases including atopic dermatitis, pneumonia, extreme pyrexia,
63 purpura fulminans, and toxic shock syndrome *(12)*. The commonly accepted model of the role of SAgs
64 in SAIE includes localized or systemic superantigenicity that causes dysregulation of the immune
65 system preventing clearance of *S. aureus* from the infected heart endothelium. SAgs also cause capillary
66 leak and hypotension which changes the hemodynamics of the vascular system *(12)*. This alteration of
67 blood flow may enhance vegetation formation. However, the requirement of superantigenicity in the
68 pathogenesis and pathophysiology of SAIE has not been directly tested. In this study, we addressed the
69 hypothesis that superantigenicity promotes SAIE and disease sequelae.
70 We used the rabbit model of native valve IE with the well-characterized methicillin-resistant *S.*
71 *aureus* strain MW2 (SEC^+) and MW2 stably expressing SEC toxoids (TCR or MHC-II/TCR inactivated)
72 to provide evidence that SEC critically contributes to vegetation growth, the magnitude of myocardial
73 inflammation, and injury to the renal and hepatic systems independent of superantigenicity. We
74 demonstrate that development of septic vegetations are a pre-requisite for decreased renal function,
75 while superantigenicity resulting from SAIE exacerbates hepatocellular injury and systemic toxicity.
76 With the use of the *ex vivo* rabbit aortic ring model of angiogenesis and human aortic endothelial cells,

77 we provide evidence that SEC inhibits re-vascularization and inhibits expression of Vascular Endothelial
78 Growth Factor (VEGF)-A, a potent pro-angiogenic factor. These results demonstrate that SEC is an
79 antiangiogenic virulence factor that directly modifies endothelial cell function by a mechanism that can
80 promote SAIE and its associated systemic pathologies.
81
82 ***S. aureus* MW2 expressing SEC toxoids are deficient in superantigen activity *in vitro* and *in vivo***
83 SAg activity is the most potent biological function of staphylococcal enterotoxins described to
84 date and causes lethal pathologies. To establish whether superantigenicity promotes development of
85 SEC-mediated SAIE, we complemented *S. aureus* MW2Δ*sec* to produce SEC with an inactive T-cell
86 receptor (TCR)-binding site (SEC_{N23A}) or to produce SEC with dual inactivation of the TCR- and MHC
87 class II-binding sites ($SEC_{N23A/F44A/L45A}$) (Table S1-S2). Due to its biological inactivation, SEC_{N23A} and
88 mutations thereof are excluded from the CDC select agent toxins *(15)*. Importantly, several vaccination
89 studies have shown no disruption in SEC_{N23A} toxin structure and in the antigenic nature of the protein
90 *(16–19)*. MHC-II is expressed by non-hematopoietic cells such as epithelial cells and endothelial cells
91 *(13)*. Hence, to exclude the possibility that interactions with MHC-II may promote disease, we
92 introduced two mutations (F44A/L45A) into SEC_{N23A} previously shown to effectively inactivate MHC-
93 II binding *(18–21)*. *S. aureus* expressing SEC_{N23A} or $SEC_{N23A/F44A/L45A}$ were confirmed to produce SEC
94 toxoids at similar levels as wildtype SEC (Fig. S1A and B) and to exhibit no defects in growth in liquid
95 culture (Fig. S1C) or defects in hemolytic activity as proxy for assessing functionality of the Agr system
96 (Fig. S1D and E).
97 To provide evidence that *S. aureus* expressing toxoids are deficient in SEC superantigenicity,
98 cell-free supernates from overnight cultures of MW2 (*S. aureus* SEC^{+}), the isogenic deletion strain
99 MW2Δ*sec* (*S. aureus* SEC^{KO}), and *S. aureus* expressing toxoids (*S. aureus* SEC_{N23A} and *S. aureus*
100 $SEC_{N23A/F44A/L45A}$) were tested in a T cell proliferation assay. For this, human peripheral blood
101 mononuclear cells (PBMCs) from 3 donors were cultured in the presence of 0.3, 2, or 10-µl volumes of
102 supernates and the replication index of $CD4^{+}$ T cells calculated 6 days post-exposure. Purified SEC (10

103 μg) was used as proliferation control. As expected, *S. aureus* SEC_{N23A} and *S. aureus* $SEC_{N23A/F44A/L45A}$
104 were both deficient in SEC superantigenicity as T cell proliferation was reduced to levels at or below
105 those resulting from *S. aureus* SEC^{KO} (Fig. 1A and Fig. S2). Similarly, the serum from rabbits infected
106 with *S. aureus* SEC_{N23A} or $SEC_{N23A/F44A/L45A}$ in the native valve IE model exhibited significantly
107 decreased concentrations of IL-6 and lactate dehydrogenase (LDH) compared to those infected with *S.*
108 *aureus* SEC^{+} (Fig. 1B and C). IL-6 is a cytokine produced at high levels as a result of superantigen
109 activity *(22)*. LDH, found in almost every cell in the body, is released into the systemic circulation as a
110 result of tissue injury including the cytotoxic effects of cytokine storms *(23–25)*. On average, both IL-6
111 and LDH levels in rabbits infected with *S. aureus* expressing toxoids were not significantly different
112 than those in rabbits infected with *S. aureus* SEC^{KO} (Fig. 1B and C). These results are consistent with
113 inactivation of superantigen activity in SEC_{N23A} and $SEC_{N23A/F44A/L45A}$ and provide further evidence of
114 deficient superantigen activity of *S. aureus* expressing toxoids.
115
116 **Superantigenicity is not sufficient to promote vegetation formation and high lethality**
117 *S. aureus* SEC^{+}, *S. aureus* SEC^{KO}, *S. aureus* SEC_{N23A}, and *S. aureus* $SEC_{N23A/F44A/L45A}$ were
118 tested in the rabbit native-valve IE model. Strains were inoculated intravenously with 2 – 4 $x10^{7}$ total
119 CFU after mechanical damage to the aortic valve and monitored for a period of 4 days. During that
120 period, rabbits infected with *S. aureus* SEC^{KO} had a ~66% decrease in overall vegetation formation
121 where 8/12 rabbits had no vegetations (Fig. 2A and B) and 4/12 had very small vegetations (sent to
122 pathology) with an estimated weight of 5 – 15 mg. In stark contrast, *S. aureus* SEC^{+} formed vegetations
123 in nearly all rabbits (14/15). Vegetation size ranged from 11 – 116 mg with most vegetations weighing
124 >25 mg (Fig. 2A and B). Six vegetations were sent for histopathology by a board-certified veterinary
125 pathologist. Surprisingly, complementation with SEC_{N23A} or $SEC_{N23A/F44A/L45A}$ restored vegetation
126 formation to wild type levels in most rabbits, with vegetation sizes ranging from 12 – 103 mg for
127 SEC_{N23A} (in 13/17 rabbits) and 3 – 107 mg for $SEC_{N23A/F44A/L45A}$ in 12/17 rabbits (Fig. 2A and B).
128 Altogether, infection with *S. aureus* expressing toxoids produced vegetations in 74% of rabbits (25/34),

129 compared to 93% (14/15) in rabbits infected with *S. aureus* SEC^{+}. Vegetations formed by *S. aureus*
130 SEC_{N23A} and *S. aureus* $SEC_{N23A/F44A/L45A}$ also had bacterial counts comparable to the wildtype strain
131 (Fig. 2C). Consistent with the contribution of vegetation formation to lethal systemic complications,
132 infection with either *S. aureus* SEC_{N23A} or *S. aureus* $SEC_{N23A/F44A/L45A}$ led to high lethality, with ~50% of
133 rabbits succumbing to infection during the experimental period compared to 73% of rabbits infected
134 with *S. aureus* SEC^{+} (Fig. 2D). Rabbits infected with *S. aureus* expressing toxoids also exhibited higher
135 degrees of splenomegaly (Fig. 2E) and on average higher bacteremia (>$1x10^3$ CFU/ml) than those
136 infected with *S. aureus* SEC^{KO}, although only those infected with $SEC_{N23A/F44A/L45A}$ exhibited
137 significantly higher bacteremia (Fig. 2F). Overall, there is an ~20% decrease in vegetation formation and
138 lethality in rabbits infected with strains producing toxoids. Thus, superantigenicity alone does not fully
139 account for the high lethal outcomes associated with SEC production in experimental SAIE. These
140 results highlight a critical requirement of SEC in SAIE that is independent of superantigenicity and
141 MHC class II interactions.
142
143 **Superantigenicity-independent effects drive myocardial inflammation in SAIE**
144 SAIE presents as rapidly-growing vegetative lesions resulting in the quick destruction of valvular
145 leaflets and progression of the infection into the myocardium and adjacent structures *(5)*. We then asked
146 whether SEC superantigenicity promotes extension of the vegetative lesion into the surrounding tissue
147 changing the overall cardiac pathology. To address this, we performed histopathological analyses on
148 transverse sections of hearts containing vegetations (Fig. S3 and S4, Table S3). Hearts from rabbits
149 infected with *S. aureus* SEC^{+}, *S. aureus* SEC_{N23A}, or *S. aureus* $SEC_{N23A/F44A/L45A}$ were selected randomly
150 based on presence of vegetations (mean size 6.6 ± 2 mm^2, n=15). We processed all hearts of *S. aureus*
151 SEC^{KO} infected rabbits with visible vegetations (mean size 2.7 ± 1 mm^2, n=4) and 3 hearts without
152 vegetations. We recognize there is selection bias in this case (and the data will reflect that), but we
153 wanted to learn pathologies associated with vegetation formation, including the 33% that forms in the
154 absence of SEC production. Consistent with histopathology of SAIE described in humans, *S. aureus*

155 vegetations in rabbits were composed of large aggregates of bacterial colonies interspersed in a fibrinous
156 meshwork of host factors and cell debris (Fig. S3-S4). However, the vegetative lesions were
157 heterogeneous across infection groups in presentation (location and size of bacterial clusters) and in the
158 magnitude of suppurative intracardial complications (myocardial inflammation and septic coronary
159 arterial emboli) (Fig. 3). In rabbits infected with *S. aureus* SEC^{+}, most vegetations were located on
160 aortic valve cusps and valve leaflets, with large clusters of bacteria present on the leaflets and
161 intermixed within the central core of the vegetation adjacent to the aorta. A few vegetations formed on
162 the aortic wall, were transmural (across the entire wall), and extended into the adjacent adipose tissue
163 (Fig S4A). Rabbits infected with *S. aureus*-producing SEC toxoids (SEC_{N23A} or $SEC_{N23A/F44A/L45A}$)
164 exhibited very similar histologic presentation to each other and to those infected with *S. aureus* SEC^{+}
165 (Fig S4B and C).

166 Most vegetative lesions presented with inflammation adjacent to the vegetations that was almost
167 exclusively heterophilic (neutrophilic) (Fig. 3A). Foci of heterophils infiltrating the myocardium,
168 cellular debris, and necrosis were also observed (Fig. 3A, insets). In the most severe cases (Grade 3),
169 large and coalescing bands of heterophilic infiltrates surrounded the aortic ring (Fig. 3A). Vegetative
170 lesions from *S. aureus* SEC^{+} consistently showed high grade myocardial inflammation that were
171 indistinguishable histologically from those formed by *S. aureus* producing SEC toxoids (SEC_{N23A} or
172 $SEC_{N23A/F44A/L45A}$) (Fig. 3B). Surprisingly, the *S. aureus* SEC^{KO} vegetations that formed on the aortic
173 wall, albeit small, caused multifocal inflammation adjacent to the vegetation (Fig. 3B and S3A). This is
174 in stark contrast to the histopathology from rabbits infected with *S. aureus* SEC^{KO} with no vegetations,
175 which was unremarkable (Fig. S3B). Of interest, septic coronary arterial emboli (coronary arteries
176 containing fibrin or bacterial thrombi) with adjacent myocardial necrosis, and/or intravascular bacteria
177 were observed in rabbits infected with *S. aureus* SEC^{+} and *S. aureus* producing SEC toxoids but absent
178 from those infected with *S. aureus* SEC^{KO} (Fig. 3C and E). Vegetations that penetrated deeper into the
179 pericardium causing epicardial lesions and saponification (necrosis) of epicardial fat was the only other
180 cardiac complication observed in one rabbit infected with *S. aureus* SEC^{KO} (Fig. 3D and E). These

181 observations indicate that 1) intracardial complications associated with embolic events result from the
182 formation of large vegetations produced in the presence of SEC, 2) myocardial inflammation, and its
183 extent, are a direct result of the presence of a vegetation, and 3) these events are largely independent of
184 SEC superantigenicity.
185
186 **Superantigenicity differentially contributes to renal and hepatic complications in SAIE**
187 Vegetation fragmentation and metastatic infection occur in one third of SAIE episodes and are
188 associated with hemodynamic and embolic complications in multiple organ systems, including the
189 vascular, pulmonary, gastrointestinal, renal, and hepatic systems *(3)*. We had previously observed renal
190 ischemia, infarction, and abscess formation associated with SEC production during SAIE in rabbits *(10)*.
191 It remains to be established whether superantigenicity-mediated toxicity significantly contributes to
192 acute kidney and liver injury during SAIE. To address these, experimental rabbits were assessed for
193 kidney and liver lesion pathology. The kidney lesions presented as hemorrhagic, necrotic, or ischemic
194 (Table S3). In the most severe pathology (Grade 3), lesions extended across a large surface of the kidney
195 (Fig. 4A). Kidneys from *S. aureus* SEC^{+} infected rabbits presented with severe pathology in 66% of the
196 animals (Fig. 4B). Similar kidney pathology developed in ~50% of rabbits infected with *S. aureus*
197 producing SEC toxoids (Fig. 4B). Although we did note that Grade 3 pathology was observed only in
198 ~25% of this group, serum levels of blood urea nitrogen (BUN) and creatinine (both biological markers
199 of decreased renal function) were significantly increased in all groups infected with SEC-producing
200 strains compared to SEC^{KO} (Fig. 4C and D).
201 Histologic analyses of kidney lesions showed that lesions were associated with ischemia and
202 smaller foci of necropurulent inflammation (Fig. 4E). Most lesions from *S. aureus* SEC^{+}-infected
203 kidneys contained more than 5 foci of necropurulent inflammation (Fig. 4F), infarctions (areas of
204 ischemic necrosis) with intralesional bacteria in either one or more of these foci of necrosis,
205 intravascular bacteria, and bacterial thrombi (Fig. 4G). Lesions induced by SEC toxoids were
206 indistinguishable histologically from those formed by *S. aureus* SEC^{+} (Fig. 4F). Of interest, lesions from

207 *S. aureus* SEC^{KO}-infected kidneys, while exhibiting high grade inflammation (Fig. 4F), failed to exhibit
208 infarction, thrombi, and intravenous bacteria (all signs of embolic events) (Fig. 4G). Hence, SEC-
209 mediated acute kidney injury is largely a result of vegetation formation and fragmentation rather than
210 kidney failure that typically results from toxic shock syndrome *(12)*.
211 Liver pathology presented grossly as pale, streak-shaped ischemic lesions that were focal,
212 multifocal, or wide-spread (Fig. 5A, Table S3). Livers from *S. aureus* SEC^{+} infected rabbits presented
213 with high grade pathology in 80% of the animals (Fig. 5B). Similar liver pathology developed in ~70%
214 of rabbits infected with *S. aureus* producing SEC toxoids (Fig. 5B). Interestingly, rabbits infected with
215 *S. aureus* SEC^{+} had significantly increased mean levels of serum AST (236 U/L) compared to the AST
216 concentration from rabbits infected with *S. aureus* producing SEC toxoids or *S. aureus* SEC^{KO} (AST ≤
217 73 U/L) (Fig. 5C). Correspondingly, the ratio of AST to ALT was significantly higher in rabbits infected
218 with *S. aureus* SEC^{+} (Fig. 5D). These increases in liver aminotransferase enzymes are consistent with
219 what is observed in humans during acute liver injury and ischemic hepatitis *(26, 27)*. As with the
220 kidneys, ischemic liver lesions were commonly associated with embolic events. Histologic analyses
221 showed ischemic necrosis (well demarcated zones of coagulation necrosis), often surrounded by
222 necropurulent inflammation and/or hemorrhage, and more diffuse centrilobular vacuolation and/or
223 necrosis (indicative of ischemia on a more global scale of the organ) (Fig. 5E and F). It is intriguing that
224 liver lesions from rabbits infected with *S. aureus* SEC^{KO} exhibited high prevalence of infarction and
225 necrosis, when heart and kidney lesions were mostly devoid of embolic complications. It is almost as if
226 the liver was the primary site of infection. Altogether, the data indicate that in addition to the embolic
227 events resulting in localized tissue injury, liver sensitivity to the toxic effects of superantigen activity
228 significantly increases hepatocellular injury.
229
230 **SEC inhibits neovessel formation in rabbit aortic explants**
231 SEC promoting SAIE and lethal systemic complications largely independent of superantigenicity
232 centers its pathophysiologic effects directly on the endothelium. In acute IE, vegetative lesions develop

233 rapidly with no evidence of repair *(28)*. This is followed by fragmentation and septic embolization of
234 cardiac vegetations leading to tissue injury and organ dysfunction, increasing mortality in patients with
235 IE *(29)*. Therefore, SEC targeting of endothelial cell function in vascular repair and re-vascularization of
236 injured/ischemic tissues may be central to both localized and systemic pathologies characteristic of
237 SAIE. Angiogenesis is the complex, coordinated process of vascular formation, critical to capillary
238 development and tissue remodeling after injury *(30, 31)*. To assess SEC effects on vascular regeneration
239 in a physiologically relevant context, we utilized the *ex vivo* rabbit aortic ring model, which preserves
240 the vessel microenvironment. Ring sections dissected from excised thoracic and abdominal aortas were
241 embedded into a basement membrane matrix to induce angiogenic sprouting along severed edges. Rings
242 were cultured under toxin conditions (SEC_{N23A}), antiangiogenic conditions (axitinib), or proangiogenic
243 conditions (basal medium with growth supplements) for 14 days. SEC_{N23A} was used in our *in vitro*
244 studies because: 1) the endothelium does not express TCR, and 2) SEC is a select agent toxin that we
245 can only modify in the SEC_{N23A} background for follow-up studies. Axitinib is an antiangiogenic
246 molecule due to its ability to inhibit signaling via the VEGF-A receptors-1, -2, and -3 thereby preventing
247 VEGF-A overexpression in endothelial cells *(32)*. VEGF-A is the most potent pro-angiogenic growth
248 factor *(33, 34)*.

249 In the rabbit aortic ring model of angiogenesis, evidence of microvessel sprouting was observed
250 between days 3-5 in rings maintained in supplemented basal media, with sprouts elongating and
251 branching over 14 days (Fig. 6A, top panels). Of interest, abdominal rings displayed denser microvessel
252 networks with a sprout surface area of 24 ± 1.8 mm^2 compared to thoracic rings which exhibited a
253 surface area of 15 ± 2.1 mm^2 (Fig. 6A, top panels). As expected, rings treated with the antiangiogenic
254 molecule axitinib failed to sprout (Fig. S5A). For SEC_{N23A}-treated rings, the dose-response analysis
255 showed significant inhibition of sprouting from both thoracic and abdominal aortic rings (Fig. 6B). At
256 the lowest treatment dose of 2.5 μg, SEC_{N23A} significantly decreased the thoracic-ring sprouting area by
257 ~93% over time and the abdominal-ring sprouting area by ~72% (Fig. 6B). Regardless of aortic origin,
258 sprouts that formed on SEC_{N23A} treated rings were detected by day 7 but their further development was

259 stunted (Fig. 6C and D; Fig. S5A and C). These results provide evidence that SEC is an antiangiogenic
260 virulence factor with the potential to effectively inhibit vascular and tissue regeneration by interfering
261 with neovessel formation.
262

263 **SEC inhibits expression of the proangiogenic factor VEGF-A in human aortic endothelial cells**

264 Re-vascularization and vascular injury repair mechanisms are driven by pro-angiogenic factors
265 released by injured tissues *(30, 31)*. Hence, we sought to establish whether SEC modifies the angiogenic
266 response in endothelial cells by altering expression of angiogenesis-related genes. To do so, we profiled
267 the expression of 24 genes important in driving multiple steps of the angiogenic response by RT-qPCR
268 (Table S4). Expression was assessed in immortalized human aortic endothelial cell (iHAEC) at 2, 4, and
269 6 h under toxin conditions (lipopolysaccharide [LPS] or SEC_{N23A}), angiogenesis-enhancing conditions
270 (VEGF-A), or angiogenesis-inhibiting conditions (axitinib). The gene expression profiles were
271 expressed as fold-change from media control, with a cut-off of ≥2-fold or ≤-2-fold as thresholds for
272 100% increases or decreases in expression levels, respectively. iHAECs grown in standard endothelial
273 cell culture conditions have been shown to produce an angiogenesis protein profile consistent with cells
274 that are triggered to sprout and are therefore already under pro-angiogenic conditions *(35)*.

275 We therefore stimulated iHAECs with bacterial LPS (25 ng/ml) to induce an expression profile
276 characteristic of proinflammatory and pathological angiogenesis *(36)*. As expected, LPS-treated cells
277 exhibited a highly pro-inflammatory profile, inducing expression of genes encoding for monocyte
278 chemoattractant protein-1 (MCP-1), granulocyte-monocyte colony stimulating factor-2 (GM-CSF2), and
279 IL-8 (Fig. 7A). The effect of this proinflammatory profile is reflected on the increased gene expression
280 for factors important in extracellular matrix degradation (Serpin E1), growth and survival (Heparin-
281 Binding Epidermal-like Growth Factor [HB-EGF], VEGF-A and VEGF-C), and migration, proliferation
282 and vessel sprouting (pentraxin 3 and angiopoietin-2) (Fig. 7B). VEGF-A stimulation of iHAECs under
283 already pro-angiogenic conditions resulted in induction of its own gene expression while inhibiting
284 genes involved in inflammation, growth, migration, and proliferation (Fig. 7). These results are

285 consistent with an endothelial cell monolayer in homeostasis with no need for further growth. The
286 VEGF-A receptor inhibitor axitinib induced a highly suppressive profile, exhibiting a ≥5-fold
287 downregulation of genes important in ECM degradation (A Disintegrin and Metalloproteinase with
288 Thrombospondin Motifs 1 [ADAMTS-1]), growth and survival (acidic FGF and VEGF-A), proliferation
289 and migration (Tissue Inhibitor of Matrix Metalloproteinase 4 [TIMP-4] and thrombospondin 1), and
290 inflammation (GM-CSF2) (Fig. 7). In stark contrast, iHAECs treatment with SEC_{N23A} at non-toxic
291 concentrations (20 μg/mL; Fig. S6) induces marked inhibition of VEGF-A gene expression, also
292 observed in early time points of axitinib-treated cells (Fig. 7). These results indicate that SEC can exert
293 antiangiogenic effects by inhibiting VEGF-A expression in endothelial cells and help explain SEC_{N23A}
294 suppression of microvessel formation in the aortic ring model.
295
296 **Discussion**
297 *S. aureus* SAgs are ubiquitous among human clinical isolates and have been implicated in both
298 colonization and pathogenic mechanisms *(37)*. Although their significance as virulence factors has been
299 established, how these multifunctional SAgs specifically contribute to *S. aureus* pathogenesis has
300 become a pressing question *(38–40).* Current evidence indicates that the SAgs SEC, TSST1 and select
301 *egc* toxins play a novel and essential role in the etiology of SAIE by yet uncharacterized mechanisms
302 *(10, 11)*. Still, in SAg-mediated illnesses, superantigenicity is placed as a triggering event mediating or
303 exacerbating pathological responses during *S. aureus* infection. It has been proposed, albeit not directly
304 tested, that superantigenicity leading to hypotension and immune dysregulation allows for bacterial
305 immune evasion and persistence, while direct interaction with the heart endothelium promotes
306 endothelium dysfunction and disease progression *(10, 11, 38)*. With the use of *S. aureus* producing SEC
307 inactivated in MHC-II and/or TCR binding, we provide evidence that superantigenicity is not the
308 primary mechanism by which SEC promotes vegetation formation, cardiac toxicity, and extracardiac
309 complications such as acute kidney injury. Our results are consistent with published studies noting that
310 not all SAgs promote SAIE to the same extent *(11)*. SEG and SEN have comparable T cell mitogenic

311 activity as SEA, SEB, and TSST1 *(41, 42)*, yet they exhibit decreased efficiency in promoting SAIE.
312 Our studies highlight the critical contribution of SAgs in life-threatening pathologies by at least two
313 novel mechanisms: 1) interference with vascular injury repair, and 2) inhibition of re-vascularization of
314 injured or ischemic tissues.

315 During SAIE, vascular injury results from mechanical damage and/or toxin-mediated damage of
316 the endothelium. Re-endothelialization of injured vessels restores their integrity and is essential to limit
317 the progressive loss of the endothelial layer and continual deposition of host factors (e.g. platelets,
318 fibrin, leukocytes) that leads to mural thrombus formation *(37)*. In the case of SAIE, re-
319 endothelialization defects would promote expansion of the vegetative lesion and growth of the
320 vegetation. We have previously shown that the SAg TSST1 directly causes dysregulated activation of
321 iHAECs and disrupts re-endothelialization in an *in vitro* wound-healing assay, suggesting a role of SAgs
322 in endothelial dysfunction and a possible explanation for their role in SAIE *(38)*. Both re-
323 endothelialization and sprout elongation are a function of cell proliferation and migration, and their
324 impairment results in angiogenesis defects *(43)*. Angiogenesis is a highly complex multistep process
325 requiring endothelial cell activation, basement membrane degradation, sprout formation and elongation,
326 and capillary network stabilization *(30, 31)*. These processes are also supported by endothelium-
327 associated cells, such as pericytes, fibroblasts, monocytes, and smooth muscle cells *(44, 45)*. These cell
328 types are not present in standard monoculture *in vitro* wound healing assays. For the study of
329 angiogenesis, the *ex-vivo* rabbit aortic ring model is a more physiologically relevant model *(30, 46)*.
330 With this model, we provide conclusive evidence that SEC disturbs branching microvessel formation,
331 effectively inhibiting angiogenesis.

332 We propose that SEC inhibition of angiogenesis occurs via a mechanism dependent on down-
333 regulation of one of the most potent inducers of angiogenesis, VEGF-A *(33, 34, 47, 48)*. VEGF-A is a
334 proangiogenic growth factor produced in virtually all vascularized tissues *(33, 48)*. It promotes
335 endothelial cell survival and mitogenic stimuli *(49, 50)*, re-endothelialization of denuded arterial walls to
336 restore the integrity of the endothelium *(51)*, and growth of new capillaries to restore perfusion to

337 ischemic tissues *(52, 53)*. Physiological levels of VEGF-A maintain vascular homeostasis and are
338 vasculoprotective, while VEGF-A up-regulation is critical to trigger sprouting angiogenesis and wound
339 repair mechanisms *(54–56)*. We provide evidence that SEC inhibits expression of *VEGFA* in iHAECs.
340 This inhibition peaks between 2 – 6 hours after SEC exposure. Similar inhibition is observed in cells
341 exposed to axitinib, a potent inhibitor of the VEGF-A receptor *(32)*. Inhibition of the VEGF-A signaling
342 pathway, regardless of the mechanism (e.g. VEGF-A neutralization or VEGF-receptor inhibition),
343 results in endothelial dysfunction and vascular toxicity, including thrombosis, inappropriate pruning of
344 the arterial vasculature, and re-vascularization defects during ischemic injury *(57–59)*. These events can
345 help explain the pathophysiology typical of SAIE.

346 SAIE has a high mortality rate owing to the high incidence of both intracardiac complications
347 arising from the rapid local spread of the infection and the high incidence of embolization of septic
348 vegetation fragments *(1, 3, 60)*. Lodging of septic emboli within terminal blood vessels causes localized
349 ischemia and infarction in multiple organ systems. In humans and in experimental rabbits, these
350 complications can be manifested as myocardial infarction, kidney and/or liver injury, and strokes *(60)*.
351 Of these, kidney injury leading to acute renal insufficiency with progression to acute renal failure is
352 tightly associated with SAIE severity, development of septic shock, and IE lethality *(7)*. Our study
353 demonstrates that SEC-associated kidney injury is a consequence of its role in vegetation formation and
354 embolization of cardiac vegetations. The kidney lesions observed upon examination ranged from
355 ischemic or hemorrhagic to necrotic. In this context, VEGF-A deficits and angiogenesis defects in
356 general can lead to persistent vascular injury and insufficient re-vascularization, overall impairing the
357 wound healing process allowing for renal deterioration and bacterial growth. The liver has central roles
358 in clearing circulating bacteria and their toxins and is key in initiating or amplifying inflammatory
359 responses during systemic infections *(7)*. Yet, literature on the effects of SAIE on liver injury is scarce
360 *(3)*. In our study, increases in serum aminotransferases correlates with increases in IL-6 and LDH in
361 rabbits infected with *S. aureus* SEC^{+}. Therefore, in contrast to the kidneys, in the liver, superantigenicity
362 significantly contributes to cellular injury.

363 Our current understanding of SAg involvement in the pathogenesis of many life-threatening *S.*
364 *aureus* infections such as bacteremia, pneumonia, and IE has been tied to complications arising from the
365 extreme effects of superantigen activity. While adaptive immune system activation is the hallmark of
366 staphylococcal SAgs, we provide evidence that this is not their only biological function involved in
367 promoting life-threatening disease pathologies. It is clear that SAgs do much more than previously
368 anticipated or expected. Therefore, it becomes fundamental to further understand the involvement of
369 superantigenicity-independent mechanisms in other invasive and life-threatening diseases as well.
370 Recently, the SAg SE*l*-X was found to inhibit neutrophil function via a sialic acid-binding motif
371 uniquely present in this SAg *(40)*. Meanwhile, TSST1 was reported to induce activation of epithelial
372 cells through a dodecapeptide close to the base of the central α- helix of the molecule *(39)*. The
373 dodecapeptide sequence is found in all staphylococcal SAgs, yet its effects on non-hematopoietic cells is
374 poorly characterized *(12, 39, 61)*. The relevance of the SEC dodecapeptide in endothelial cell function
375 and *S. aureus* diseases such as IE is not known but it is at the center of current studies.
376 Altogether, our study demonstrates that superantigenicity independent effects of SEC are
377 essential to the pathogenesis and pathophysiology of SAIE. The data further shows that SEC is an anti-
378 angiogenic toxin that inhibits sprouting of new capillaries from the activated endothelium, which would
379 effectively impair re-vascularization of injured tissues. It is becoming evident that SAgs like TSST1 and
380 SEC promote IE by interfering with vascular repair and the angiogenic process. One of the mechanisms
381 by which SEC may exert its anti-angiogenic effects is through the inhibition of endothelial cell
382 expression of one of the key inducers of angiogenesis, VEGF-A. If so, deficient angiogenesis may be at
383 the center of many pathologies associated with SAg-producing *S. aureus* infections. Given the reach of
384 the vascular endothelium into every organ system and the prevalence of SAgs among both methicillin-
385 susceptible and resistant *S. aureus* strains, SAgs have the potential to promote pathologies in every
386 organ that they encounter.
387
388

389 **Materials and methods**

390 **Bacterial strains and growth conditions**

391 Community-associated, methicillin-resistant USA400 strain MW2 was originally obtained in the
392 Upper Midwest from a young patient who succumbed to necrotizing pneumonia. *S. aureus* MW2
393 encodes for the SAgs SEC, SEA, SEH, SEK, SEL, SEQ, and SE-*like* X. SEC is produced at 60-100
394 μg/ml in liquid culture, while the rest are produced at 0.0001-0.03μg/ml. Staphylococcal strains were
395 used from low-passage-number stocks. All staphylococcal strains were grown in Bacto™ Todd Hewitt
396 (TH) (Becton Dickinson) broth at 37°C with aeration (225 rpm) unless otherwise stated. Strains and
397 plasmids used in this study are listed in Table S1. Plasmids used for complementation were maintained
398 using carbenicillin (100 μg/ml) in *E. coli* DH5α. For endocarditis experiments, strains were grown
399 overnight, diluted, and washed in phosphate buffered saline (PBS - 2mM NaH_2PO_4, 5.7 mM Na_2HPO_4,
400 0.1 M NaCl, pH 7.4).

401

402 **Selection of mutations inactivating the SEC TCR binding site (N23A) or the MHC-II binding site**
403 **(F44A/L45A)**

404 Asn^{23} is a highly-conserved, surface exposed residue located in a cleft between the O/B fold and
405 β-grasp domain of SAgs *(62)*. It forms hydrogen bonds with the backbone atoms of the
406 complementarity-determining region (CDR) 2 of the Vβ-TCR *(63)*. As such, Asn^{23} contact with the Vβ-
407 TCR has one of the greatest energetic contributions of the complex. Mutations in this position, such as
408 N23A or N23S, greatly destabilize the Vβ-TCR:SAg interaction with profound effects in SAg activity
409 *(63)*. SEC_{N23A} has no detectable binding to Vβ-TCR as measured by surface plasmon resonance, no
410 proliferative T-cell responses in thymidine-incorporation assays at concentrations up to 30 μg/ml *(63)*,
411 no lethality or signs of TSS in rabbits vaccinated subcutaneously with 25 μg three times every two
412 weeks *(16)*, and no lethality in rabbits after intravenous injection at 3,000 μg/kg *(15)*. Phe^{44} and Leu^{45},
413 conserved among all enterotoxins, are located on a protruding hydrophobic loop that directly contacts
414 MHC-II and forms strong electrostatic interactions with the α-chain *(20, 64)*. Leu^{45} is the most

415 extensively buried amino-acid residue in the SEC:MHC-II interface, but mutations in either residue
416 (Phe[44] or Leu[45]) effectively inactivate SEC binding *(18–21, 64)*. F44S alone is 1000-fold less efficient in
417 MHC-II binding resulting in a concomitant reduction of IL-2 in T-cell proliferation assays *(19, 65)*.
418

419 **Construction of chromosomally complemented toxoid strains**

420 SEC is a CDC designated select agent. As such, we are not allowed to use the wildtype copy of
421 the gene in recombinant studies. For this reason, all PCR products generated in the making of the toxoid
422 complement strains either included the permissible N23A mutation or was only a partial amplification of
423 *sec* missing either the TCR or MHC-II domain. Each step of plasmid construction was verified by
424 Sanger sequencing to contain the N23A TCR mutation. PCR amplification was performed using Phusion
425 polymerase (New England Biolabs; NEB) unless otherwise noted. *S. aureus* expressing SEC_{N23A} or
426 $SEC_{N23A/F44A/L45A}$ were made by markerless chromosomal complementation in MW2Δ*sec* with the genes
427 expressed under the control of the native promoter and terminator *(66)*. The SEC_{N23A} gene sequence was
428 created by amplifying two fragments from MW2 with primer sets pJB38xN23ApromF/promN23R and
429 termN23F/pJB38xN23AtermR. The chromosomal complementation plasmid, pJB38-NWMN29-30
430 (RRID:Addgene_84457), was digested with EcoRV and PCR products inserted by Gibson Assembly
431 (NEB) as previously described, creating pKK29 *(67)*. SEC_{N23A} was amplified from pKK29 with the
432 primer set pUC19SECN23AptF/pUC19SECN23AptR and inserted by Gibson Assembly into pUC19
433 (RRID:Addgene_50005) linearized with KpnI and EcoRI, to create pKK33. The MHC-II binding site
434 mutations were introduced into pKK33 by site-directed mutagenesis (QuickChange II, Agilent
435 Technologies) using the primer set SECF44A/L45Afor/ SECF44A/L45Arev, creating pKK39. The
436 $SEC_{N23A/F44A/L45A}$ gene sequence was amplified from pKK39 with primer set pJB38xN23ApromF/
437 pJB38xN23AtermR and inserted into pJB38-NWMN29-30 as described above, creating pKK42. pKK29
438 and pKK42 were electroporated into *S. aureus* RN4220 and moved into MW2Δ*sec* by generalized
439 transduction with ϕ11*(68)*. *S. aureus* strains containing plasmids were selected for with
440 chloramphenicol (20 µg/ml) at 30°C. Allelic exchange was performed as previously described *(66)*,

441 chromosomal insertions detected by PCR with primer set XNWMN2930F/XNWMN2930R, and verified
442 by Sanger sequencing. Primers were purchased from Integrated DNA Technologies (Table S2).
443
444 **SEC purification and T cell proliferation assay**
445 SEC was purified from *S. aureus* strain FRI913 in its native form by ethanol precipitation and
446 thin-layer isoelectric focusing as previously described *(69)*. Preparation of SEC resulted in a single band
447 by Coomassie blue stain. Toxin preparations were tested for lipopolysaccharide (LPS) contamination
448 with the Toxin Sensor Chromogenic LAL Endotoxin Assay following the manufacturer's instructions
449 (GenScript). SEC preparations had < 0.02 ng of LPS per 20 µg of SEC^{+}. For analysis of superantigen
450 activity in *S. aureus* expressing SEC_{N23A}, $SEC_{N23A/F44A/L45A}$, SEC, or SEC^{KO}, cell-free supernates were
451 collected from bacteria grown overnight, centrifuged, and filtered (0.22-µm pore size, MilliporeSigma).
452 Mononuclear cells were isolated from human peripheral blood samples (PBMC) originating from 3
453 donors by density gradient centrifugation using ficoll-paque PLUS (UW–Madison Minimal Risk IRB
454 Protocol 2018-0304-CR004). PBMCs were labelled with 5µM Cell Trace Violet (CTV) dye (Thermo
455 Fisher Scientific) following the manufacturer's protocol. CTV labelled cells were plated in 96-well
456 plates at a concentration of 2×10^4 cells/well in RPMI 1640 medium supplemented with 10% heat-
457 inactivated fetal bovine serum, 5% heat inactivated bovine calf serum, 3% human AB serum, 1% L-
458 glutamine and 1% penicillin/streptomycin. Purified SEC (10µg), or cell-free supernates at 0.3, 2, or 10-
459 µl volumes were added to the wells. After 6 days, cell division of $CD4^{+}$ T cells was assessed flow
460 cytometrically by measuring dilution of CTV fluorescence intensity. Proliferation response was
461 quantified using the FlowJo proliferation platform analysis tool and data presented as replication index
462 or percent of $CD4^{+}$ T cell divided.
463
464 **Rabbit model of SAIE**
465 The rabbit model of IE was performed as previously described with some modifications *(10)*. 2-3
466 kg New Zealand White Rabbits were obtained from Bakkom Rabbitry (Red Wing, MN) and

467 anesthetized with ketamine (dose range: 10-50 mg/kg) and xylazine (dose range: 2.5-10 mg/kg).
468 Mechanical damage to the aortic valve was done by introducing a hard, plastic catheter via the left
469 carotid artery, left to pulse against the valve for 2 h, removed, and the incision closed. Rabbits were
470 inoculated via the marginal ear vein with 2 x 10^7-4 x 10^7 total CFU in PBS and monitored 4 times daily
471 for a period of 4 days. For pain management, rabbits received buprenorphine (dose range: 0.01 – 0.05
472 mg/kg) twice daily. At the conclusion of each experiment, bacterial counts were obtained from
473 heparinized blood (50 USP units/mL). Rabbits were euthanized with Euthasol (Virbac) and necropsies
474 performed to assess overall health. Spleens were weighed and used as an infection control, kidney and
475 liver gross pathology was graded using gross lesion pathology scale (Table S3), aortic valves were
476 exposed to assess vegetation growth, and vegetations that formed were excised, weighed, and suspended
477 in PBS for CFU counts. A minimum of 4 rabbit hearts from each infection group were placed in 10%
478 neutral buffered formalin and further processed by the Comparative Pathology Laboratory at the
479 University of Iowa for histopathological analyses. Vegetation weight and bacterial counts cannot be
480 obtained from hearts prepared for histology. Experiments were performed according to established
481 guidelines and the protocol approved by the University of Iowa Institutional Animal Care and Use
482 Committee (Protocol 6121907). Number of rabbits per infection group were as follow: *S. aureus* SEC^{+}
483 (n=12), *S. aureus* SEC^{KO} (n=15), *S. aureus* SEC_{N23A} (n=17), and *S. aureus* $SEC_{N23A/F44A/L45A}$ (n=17).
484 Data from rabbit experimental groups are a result of at least 3 independent experiments.
485

486 **Serum analysis**

487 Rabbit serum was obtained from heparinized blood (50 USP units/mL) collected before infection
488 and at 48 h, 72 h, and 96 h post infection. Blood was centrifuged at room temperature at 5000 x g for 10
489 min. The collected supernatant was centrifuged for an additional 5 min, filter sterilized using a 0.2 μm
490 filter, and stored at -80°C for further analysis. Serum samples were sent to the University of Iowa
491 Diagnostic Laboratories and evaluated for the following serum analytes: aspartate aminotransferase
492 (AST; U/L), alanine aminotransferase (ALT; U/L), blood urea nitrogen (BUN; mg/dl), creatinine

493 (mg/dl), and lactate dehydrogenase (LDH; mg/dl). IL-6 was quantified from serum samples using the
494 R&D Systems DuoSet Rabbit IL-6 ELISA kit according to manufacturer's instructions. Serum samples
495 were diluted 1:10 in reagent diluent prior to use. The optical density (O.D.) was determined using a
496 TECAN M200 plate reader (Tecan Group Ltd.) set to 450 nm with wavelength correction set to 540 nm.
497 A standard curve was created by linear regression analysis of the IL-6 concentration versus O.D., log-
498 transformed (GraphPad Prism 8).
499

500 **Histopathology scoring**

501 Fixed tissues were routinely processed, cut at 5 µm, and hematoxylin and eosin (H&E) stained or
502 Gram stained. The slides were scored in a semi-blinded fashion, with the pathologist only made aware of
503 control animals. Histopathologic scoring was developed specifically for this animal model, as outlined
504 in Gibson-Corley et. al, 2013 *(70)* and explained in Table S3. Rabbits infected with *S. aureus* SEC^{KO}
505 with no vegetations did not exhibit pathology at the end of experimentation (n=3). Hence, all hearts of *S.*
506 *aureus* SEC^{KO} infected rabbits with visible vegetations were processed (mean size 2.7 ± 1 mm^2, n=4).
507 Heart, kidney and liver sections from rabbits infected with *S. aureus* SEC^{+}, *S. aureus* SEC_{N23A}, and *S.*
508 *aureus* $SEC_{N23A/F44A/L45A}$ were selected randomly based on presence of vegetations (mean size 6.6 ± 2
509 mm^2, n=15) and gross pathology lesions in the kidney and liver.
510

511 **SEC_{N23A} expression and purification**

512 SEC_{N23A} (C-terminus 6xHis-tagged) was expressed in *E. coli* BL21 (DE3) Star strain harboring
513 pET25bHSVdelTEV. Following ethanol precipitation, toxins were purified through Ni^{2+}-affinity
514 chromatography using a HiTrap Heparin HP column (GE Healthcare). Protein capture was verified via
515 visualization of a single band on SDS-PAGE following Coomassie blue staining. Detoxi-Gel endotoxin
516 removing resin (Thermo Scientific) was used to reduce LPS contamination to <0.001ng of LPS per 30µg
517 of toxin was obtained. Endotoxin levels were quantified using ToxinSensor™ Chromogenic LAL
518 Endotoxin kit (GenScript) to ensure toxin purity.

519 ***Ex-vivo* rabbit aortic ring model of angiogenesis**

520 Mixed-sex New Zealand white rabbits, 2-3 kg, were purchased from Charles River Laboratories
521 (Massachusetts) and maintained at Charmany Instructional Facility at the School of Veterinary Medicine
522 (SVM) of the University of Wisconsin–Madison, according to established guidelines and the protocol
523 approved by the Institutional Animal Care and Use Committee (Protocol V006222-A02). Aortic ring
524 explants were cultured by modifying the thin-layer method *(71)*. Briefly, the thoracic and abdominal
525 aortas were excised immediately after euthanasia, cleaned to remove excess fascia and connective tissue,
526 dissected into 1 – 1.5 mm cross-sections, and embedded into GFR-Matrigel coated wells (200 µL phenol
527 red-free Corning® Matrigel® Growth Factor Reduced (GFR) Basement Membrane Matrix) in a 48-well
528 plate format. After 10 min polymerization at 37°C, 5% CO_2, 200-µL supplemented Medium 200 was
529 added and plates incubated at 37°C, 5% CO_2 for up to 14 days. Medium 200 contained LSGS (see
530 Human aortic endothelial cell culture and RNA extraction), 100 U mL^{-1} penicillin-streptomycin, 2.5 µg
531 mL^{-1} amphotericin B, and designated treatment. Media (± treatments) was changed every 3-5 days.
532 Rings were treated with SEC_{N23A} at 2.5, 5, 10, and 20 µg and axitinib at 10 µM. Rings treated initially
533 with 20 µg were switched to 10 µg following the first media change to maintain toxin pressure while
534 limiting potential cytotoxic effects. Equal numbers of thoracic and abdominal aortic rings were used for
535 each treatment condition as follows: media control (n=24), axitinib (n=8), SEC_{N23A} 2.5 µg (n=6),
536 SEC_{N23A} 5 µg (n=9), SEC_{N23A} 10 µg (n=9), and SEC_{N23A} 10 µg (n=8). All treatment conditions were
537 assessed from 3 separate rabbits with the exception of SEC_{N23A} at 2.5 µg, which was completed in 2
538 rabbits. Phase-contrast images were captured on days 0, 7, and 14 with the Leica DMi8 equipped with a
539 Tokai Hit stage-top incubator set to 37°C, 5% CO_2 using a HC PL FLUOTAR 4x/0.13 objective lens.
540 Sprouting was assessed using ImageJ *(72)*.

541

542 **Human aortic endothelial cell culture and RNA extraction**

543 Immortalized human aortic endothelial cells (iHAECs) are a recently established cell line shown
544 to retain phenotypic and functional characteristics of primary cells *(38)*. iHAECs were cultured at 37°C,

545 5% CO_2 in phenol red–free, endothelial cell basal medium (Medium 200) supplemented with low-serum
546 growth supplement (LSGS, final concentrations of: FBS 2%, hydrocortisone 1μg mL^{-1}, human
547 epidermal growth factor 10 ng mL^{-1}, basic fibroblast growth factor, 3 ng mL^{-1}, heparin 10 μg mL^{-1}), both
548 from Gibco Life Technologies), as previously described *(38)*. LSGS contains the final concentrations of:
549 FBS 2%, hydrocortisone 1μg mL^{-1}, human epidermal growth factor 10 ng mL^{-1}, basic fibroblast growth
550 factor, 3 ng mL^{-1}, heparin 10 μg mL^{-1}). All experiments were conducted with iHAECs at passages 4-10
551 from a single clone seeded at 5 x 10^5/well in a 6-well plate. iHAECs were treated with LPS (25 ng mL^{-}
552 ^{1}), VEGF-A (20 nM), axitinib (25 nM), or SEC (20 μg mL^{-1}) for 2, 4, and 6 h. Data are the result of
553 three biological replicates. RNA was extracted at the indicated time points using the miRNeasy Mini Kit
554 (Qiagen), according to the manufacturer's instructions, and stored at –80°C. Contaminating genomic
555 DNA (gDNA) was removed using the Turbo DNA-Free™ Kit (Invitrogen). RNA quantity and purity
556 were assessed using the NanoDrop™ 1000 (Thermo Fisher) with median A260/280 values of 1.93 and
557 A260/230 of 1.55.
558
559 **cDNA synthesis and real-time reverse-transcription PCR**
560 cDNA synthesis was carried out using DNA-free RNA with the RT First Strand Kit according to
561 manufacturer's instructions (Qiagen). Each cDNA sample was used at 120 ng/well in 96-well plates.
562 qPCR was conducted using the PowerUP SYBR Green Master Mix (ThermoFisher Scientific, USA)
563 with each reaction having 5 μL of PowerUP SYBR Green Master Mix, 2 μL of 1 μM forward and
564 reverse gene-specific primers (Table S4), and 3 μL of diluted cDNA experimental sample in a final
565 reaction volume of 10 μL. Reactions were run with the following cycle profile: initial denaturation -
566 95°C 10 minutes, 40 cycle amplification/elongation - 95°C 15 seconds followed by 60°C 1 minute.
567 gDNA contamination from each sample was assessed using a total of 120 ng of RNA (no reverse
568 transcriptase) with reaction conditions as listed above with all samples having C_T values >35. No-
569 template controls were run with each qPCR plate and had C_T values >38. All qPCR reactions were run
570 and analyzed on the QuantStudio 3 Real-Time PCR System with analysis software v1.5.1 (Applied

571 Biosystems). Each timepoint was collected in biological triplicates with qPCR reactions from each
572 experimental sample done in technical triplicates.
573
574 **Statistical analyses**
575 The log-rank, Mantel Cox test was used for statistical significance of survival curves. Normality
576 was assessed using the D'Agostino & Pearson test along with associated Q-Q plots for data distribution.
577 For comparison across means log-transformed data was used and statistical significance was determined
578 by using one-way analysis of variance (ANOVA) with Holm- Šídák's multiple comparisons test for the
579 following data sets: vegetation size, vegetation CFU, blood CFU, spleen size, BUN, creatinine, AST,
580 ALT, LDH, and IL-6. Statistical significance for gross pathology data was determined using Fisher's
581 exact test along with calculated odds ratios and 95% confidence intervals. Statistical significance for
582 sprouting area in the aortic ring model was determined by two-way ANOVA with Holm- Šídák's
583 multiple comparisons test. Statistical significance of virulence factor production was determined with
584 the nonparametric Kruskal-Wallis test. $\alpha = 0.05$ (GraphPad Prism 8).
585

586 **References**

587 1. V. G. Fowler, J. M. Miro, B. Hoen, C. H. Cabell, E. Abrutyn, E. Rubinstein, G. R. Corey, D.
588 Spelman, S. F. Bradley, B. Barsic, P. A. Pappas, K. J. Anstrom, D. Wray, C. Q. Fortes, I. Anguera, E.
589 Athan, P. Jones, J. T. M. Van Der Meer, T. S. J. Elliott, D. P. Levine, A. S. Bayer, *Staphylococcus*
590 *aureus* endocarditis: A consequence of medical progress, *J. Am. Med. Assoc.* **293**, 3012–3021 (2005).
591 2. D. H. Bor, S. Woolhandler, R. Nardin, J. Brusch, D. U. Himmelstein, Infective Endocarditis in the
592 U.S., 1998-2009: A Nationwide Study, *PLoS One* **8**, e60033–e60033 (2013).
593 3. S. Y. C. Tong, J. S. Davis, E. Eichenberger, T. L. Holland, V. G. Fowler, *Staphylococcus aureus*
594 infections: Epidemiology, pathophysiology, clinical manifestations, and management, *Clin. Microbiol.*
595 *Rev.* **28**, 603–661 (2015).
596 4. V. G. Fowler, D. T. Durack, Infective endocarditis, *Curr. Opin. Cardiol.* **9** (1994).
597 5. G. Thiene, C. Basso, Pathology and pathogenesis of infective endocarditis in native heart valves,
598 *Cardiovasc. Pathol.* **15**, 256–263 (2006).
599 6. M. L. F. Guerrero, J. J. G. López, A. Goyenechea, J. Fraile, M. De Gó rgolas, Endocarditis caused by
600 *Staphylococcus aureus* a reappraisal of the epidemiologic, clinical, and pathologic manifestations with
601 analysis of factors determining outcome, *Medicine (Baltimore).* **88**, 1–22 (2009).
602 7. C. Olmos, I. Vilacosta, C. Fernández, J. López, C. Sarriá, C. Ferrera, A. Revilla, J. Silva, D. Vivas, I.
603 González, J. San Román, Contemporary epidemiology and prognosis of septic shock in infective
604 endocarditis, *Eur. Heart J.* **34**, 1999–2006 (2013).
605 8. E. Klein, D. L. Smith, R. Laxminarayan, Hospitalizations and deaths caused by methicillin-resistant
606 *Staphylococcus aureus*, United States, 1999-2005, *Emerg. Infect. Dis.* **13**, 1840–1846 (2007).
607 9. J. J. C. Nienaber, B. K. Sharma Kuinkel, M. Clarke-Pearson, S. Lamlertthon, L. Park, T. H. Rude, S.
608 Barriere, C. W. Woods, V. H. Chu, M. Marín, S. Bukovski, P. Garcia, G. R. Corey, T. Korman, T.
609 Doco-Lecompte, D. R. Murdoch, L. B. Reller, V. G. Fowler, Methicillin-susceptible *Staphylococcus*
610 *aureus* endocarditis isolates Are associated with clonal complex 30 genotype and a distinct repertoire of
611 enterotoxins and adhesins, *J. Infect. Dis.* **204**, 704–713 (2011).

612 10. W. Salgado-Pabón, L. Breshears, A. R. Spaulding, J. A. Merriman, C. S. Stach, A. R. Horswill, M.
613 L. Peterson, P. M. Schlievert, E. J. Johnson, Ed. Superantigens are critical for *Staphylococcus aureus*
614 infective endocarditis, sepsis, and acute kidney injury, *MBio* **4**, e00494-13 (2013).
615 11. C. S. Stach, B. G. Vu, J. A. Merriman, A. Herrera, M. P. Cahill, P. M. Schlievert, W. Salgado-
616 Pabón, Novel Tissue Level Effects of the *Staphylococcus aureus* Enterotoxin Gene Cluster Are Essential
617 for Infective Endocarditis, *PLoS One* **11**, e0154762–e0154762 (2016).
618 12. A. R. Spaulding, W. Salgado-Pabón, P. L. Kohler, A. R. Horswill, D. Y. M. Leung, P. M. Schlievert,
619 Staphylococcal and streptococcal superantigen exotoxins, *Clin. Microbiol. Rev.* **26**, 422–447 (2013).
620 13. P. A. Brogan, V. Shah, N. Klein, M. J. Dillon, Vβ-restricted T cell adherence to endothelial cells: A
621 mechanism for superantigen-dependent vascular injury, *Arthritis Rheum.* **50**, 589–597 (2004).
622 14. S. W. Tuffs, S. M. M. Haeryfar, J. K. McCormick, Manipulation of Innate and Adaptive Immunity
623 by Staphylococcal Superantigens, *Pathog. (Basel, Switzerland)* **7**, 53 (2018).
624 15. Centers for Disease Control and Prevention, (CDC), Federal Select Agent Program, "Select Agents
625 and Toxins Exclusions: Nontoxic HHS toxins" (Section 73.3 (d)(2);
626 https://www.selectagents.gov/sat/exclusions/nontoxic.htm) [the easiest access to this source is via the
627 URL].
628 16. A. R. Spaulding, W. Salgado-Pabón, J. A. Merriman, C. S. Stach, Y. Ji, A. N. Gillman, M. L.
629 Peterson, P. M. Schlievert, Vaccination Against *Staphylococcus aureus* Pneumonia, *J. Infect. Dis.* **209**,
630 1955–1962 (2013).
631 17. J. Y. Choi, S. Shin, N. Y. Kim, W. S. Son, T. J. Kang, D. H. Song, C. H. Yu, G. H. Hur, S. T. Jeong,
632 Y. K. Shin, A novel staphylococcal enterotoxin B subunit vaccine candidate elicits protective immune
633 response in a mouse model, *Toxicon* **131**, 68–77 (2017).
634 18. R. G. Ulrich, M. A. Olson, S. Bavari, Development of engineered vaccines effective against
635 structurally related bacterial superantigens, *Vaccine* **16**, 1857–1864 (1998).
636 19. M. A. Woody, T. Krakauer, B. G. Stiles, Staphylococcal enterotoxin B mutants (N23K and F44S):
637 Biological effects and vaccine potential in a mouse model, *Vaccine* **15**, 133–139 (1997).

638 20. T. S. Jardetzky, J. H. Brown, J. C. Gorga, L. J. Stern, R. G. Urban, Y. I. Chi, C. Stauffacher, J. L.
639 Strominger, D. C. Wiley, Three-dimensional structure of a human class II histocompatibility molecule
640 complexed with superantigen, *Nature* **368**, 711–718 (1994).
641 21. M. A. Woody, T. Krakauer, R. G. Ulrich, B. G. Stiles, Differential Immune Responses to
642 Staphylococcal Enterotoxin B Mutations in a Hydrophobic Loop Dominating the Interface with Major
643 Histocompatibility Complex Class II Receptors, *J. Infect. Dis.* **177**, 1013–1022 (1998).
644 22. P. A. Szabo, A. Goswami, D. M. Mazzuca, K. Kim, D. B. O'Gorman, D. A. Hess, I. D. Welch, H. A.
645 Young, B. Singh, J. K. McCormick, S. M. M. Haeryfar, Rapid and Rigorous IL-17A Production by a
646 Distinct Subpopulation of Effector Memory T Lymphocytes Constitutes a Novel Mechanism of Toxic
647 Shock Syndrome Immunopathology, *J. Immunol.* **198**, 2805–2818 (2017).
648 23. J. G. Zein, G. L. Lee, M. Tawk, M. Dabaja, G. T. Kinasewitz, Prognostic Significance of Elevated
649 Serum Lactate Dehydrogenase (LDH) in Patients with Severe Sepsis, *Chest* **126**, 873S (2004).
650 24. K. Hayashida, Y. Chen, A. H. Bartlett, W. P. Pyong, Syndecan-1 is an *in vivo* suppressor of gram-
651 positive toxic shock, *J. Biol. Chem.* **283**, 19895–19903 (2008).
652 25. R. Sada, S. Fukuda, H. Ishimaru, Toxic shock syndrome due to community-acquired methicillin-
653 resistant *Staphylococcus aureus* infection: Two case reports and a literature review in Japan, *IDCases* **8**,
654 77–80 (2017).
655 26. E. G. Giannini, R. Testa, V. Savarino, Liver enzyme alteration: a guide for clinicians, *CMAJ* **172**,
656 367–379 (2005).
657 27. V. Fuhrmann, B. Jäger, A. Zubkova, A. Drolz, Hypoxic hepatitis – epidemiology, pathophysiology
658 and clinical management, *Wien. Klin. Wochenschr.* **122**, 129–139 (2010).
659 28. C. N. Gentry, J. R. McDonald, Acute infective endocarditis, *Infect. Dis. Crit. Care* **23**, 271–283
660 (2007).
661 29. T. R. Wojda, K. Cornejo, A. Lin, A. Cipriano, S. Nanda, J. D. Amortegui, B. T. Wojda, S. P.
662 Stawicki, "Septic Embolism: A Potentially Devastating Complication of Infective Endocarditis" in
663 *Contemporary Challenges in Endocarditis*, M.S. Firstenberg, Eds. (IntechOpen, 2016), chap. 8, DOI:

664 10.5772/64931.

665 30. T. H. Adair and J.-P. Montani, "Colloquium series on integrated systems physiology: from molecule
666 to function to disease," in *Angiogenesis*, D. N. Granger and J. P. Granger, Eds (Morgan & Claypool,
667 2010), Vol. 2, No. 1, Pages 1-84.

668 31. F. Moccia, S. Negri, M. Shekha, P. Faris, G. Guerra, Endothelial Ca^{2+} signaling, angiogenesis and
669 vasculogenesis: Just what it takes to make a blood vessel, *Int. J. Mol. Sci.* **20** (2019).

670 32. R. J. Kelly, O. Rixe, Axitinib-a selective inhibitor of the vascular endothelial growth factor (VEGF)
671 receptor, *Target. Oncol.* **4**, 297–305 (2009).

672 33. A. Hoeben, B. Landuyt, M. S. Highley, H. Wildiers, A. T. Van Oosterom, E. A. De Bruijn, Vascular
673 endothelial growth factor and angiogenesis, *Pharmacol. Rev.* **56**, 549–580 (2004).

674 34. P. Carmeliet, VEGF as a key mediator of angiogenesis in cancer, *Oncology* **69**, 4–10 (2005).

675 35. P. M. Tran, S. S. Tang, W. Salgado-Pabón, *Staphylococcus aureus* β-Toxin Exerts Anti-angiogenic
676 Effects by Inhibiting Re-endothelialization and Neovessel Formation*Front. Microbiol.* **13** (2022).

677 36. Y. Li, H. Zhu, X. Wei, H. Li, Z. Yu, H. M. Zhang, W. C. Liu, LPS induces HUVEC angiogenesis *in*
678 *vitro* through miR-146a-mediated TGF-β1 inhibition, *Am. J. Transl. Res.* **9**, 591–600 (2017).

679 37. K. Werdan, S. Dietz, B. Löffler, S. Niemann, H. Bushnaq, R. E. Silber, G. Peters, U. Müller-
680 Werdan, Mechanisms of infective endocarditis: Pathogen-host interaction and risk states, *Nat. Rev.*
681 *Cardiol.* **11**, 35–50 (2014).

682 38. K. Kulhankova, K. J. Kinney, J. M. Stach, F. A. Gourronc, I. M. Grumbach, A. J. Klingelhutz, W.
683 Salgado-Pabón, The Superantigen Toxic Shock Syndrome Toxin 1 Alters Human Aortic Endothelial
684 Cell Function, *Infect. Immun.* **86**, e00848-17 (2018).

685 39. A. J. Brosnahan, M. M. Schaefers, W. H. Amundson, M. J. Mantz, C. A. Squier, M. L. Peterson, P.
686 M. Schlievert, Novel toxic shock syndrome toxin-1 amino acids required for biological activity,
687 *Biochemistry* **47**, 12995–13003 (2008).

688 40. S. W. Tuffs, D. B. A. James, J. Bestebroer, A. C. Richards, M. I. Goncheva, M. O'Shea, B. A. Wee,
689 K. S. Seo, P. M. Schlievert, A. Lengeling, J. A. van Strijp, V. J. Torres, J. R. Fitzgerald, The

690 *Staphylococcus aureus* superantigen SElX is a bifunctional toxin that inhibits neutrophil function, *PLoS*
691 *Pathog.* **13** (2017).
692 41. D. Grumann, S. S. Scharf, S. Holtfreter, C. Kohler, L. Steil, S. Engelmann, M. Hecker, U. Völker, B.
693 M. Bröker, Immune Cell Activation by Enterotoxin Gene Cluster (egc)-Encoded and Non- egc
694 Superantigens from *Staphylococcus aureus* , *J. Immunol.* **181**, 5054–5061 (2008).
695 42. D. S. Terman, A. Serier, O. Dauwalder, C. Badiou, A. Dutour, D. Thomas, V. Brun, J. Bienvenu, J.
696 Etienne, F. Vandenesch, G. Lina, Staphylococcal entertotoxins of the enterotoxin gene cluster (egcSEs)
697 induce nitric oxide- and cytokine dependent tumor cell apoptosis in a broad panel of human tumor cells,
698 *Front. Cell. Infect. Microbiol.* **4**, 38 (2013).
699 43. D. A. Chistiakov, A. N. Orekhov, Y. V. Bobryshev, Endothelial barrier and its abnormalities in
700 cardiovascular disease, *Front. Physiol.* **6**, 365 (2015).
701 44. H. Gerhardt, C. Betsholtz, Endothelial-pericyte interactions in angiogenesis, *Cell Tissue Res.* **314**,
702 15–23 (2003).
703 45. D. Ribatti, E. Crivellato, Immune cells and angiogenesis, *J. Cell. Mol. Med.* **13**, 2822–2833 (2009).
704 46. V. Baeriswyl, G. Christofori, The angiogenic switch in carcinogenesis, *Semin. Cancer Biol.* **19**, 329–
705 337 (2009).
706 47. H. Takahashi, M. Shibuya, The vascular endothelial growth factor (VEGF)/VEGF receptor system
707 and its role under physiological and pathological conditions, *Clin. Sci.* **109**, 227–241 (2005).
708 48. J. A. Nagy, A. M. Dvorak, H. F. Dvorak, VEGF-A and the induction of pathological angiogenesis,
709 *Annu. Rev. Pathol.* **2**, 251–275 (2007).
710 49. J. E. Nör, J. Christensen, D. J. Mooney, P. J. Polverini, Vascular endothelial growth factor (VEGF)-
711 mediated angiogenesis is associated with enhanced endothelial cell survival and induction of Bcl-2
712 expression, *Am. J. Pathol.* **154**, 375–384 (1999).
713 50. H. P. Gerber, A. McMurtrey, J. Kowalski, M. Yan, B. A. Keyt, V. Dixit, N. Ferrara, Vascular
714 endothelial growth factor regulates endothelial cell survival through the phosphatidylinositol 3'-
715 kinase/Akt signal transduction pathway: Requirement for Flk-1/KDR activation, *J. Biol. Chem.* **273**,

716 30336–30343 (1998).

717 51. R. Hutter, F. E. Carrick, C. Valdiviezo, C. Wolinsky, J. S. Rudge, S. J. Wiegand, V. Fuster, J. J.
718 Badimon, B. V. Sauter, Vascular endothelial growth factor regulates reendothelialization and neointima
719 formation in a mouse model of arterial injury, *Circulation* **110**, 2430–2435 (2004).

720 52. J. Banbury, M. Siemionow, S. Porvasnik, S. Petras, E. Browne, Improved perfusion after subcritical
721 ischemia in muscle flaps treated with vascular endothelial growth factor, *Plast. Reconstr. Surg.* **106**,
722 1541–1546 (2000).

723 53. J. J. Lopez, R. J. Laham, A. Stamler, J. D. Pearlman, S. Bunting, A. Kaplan, J. P. Carrozza, F. W.
724 Sellke, M. Simons, VEGF administration in chronic myocardial ischemia in pigs, *Cardiovasc. Res.* **40**,
725 272–281 (1998).

726 54. G. E, Y. Cao, S. Bhattacharya, S. Dutta, E. Wang, D. Mukhopadhyay, Endogenous vascular
727 endothelial growth factor-A (VEGF-A) maintains endothelial cell homeostasis by regulating VEGF
728 receptor-2 transcription, *J. Biol. Chem.* **287**, 3029–3041 (2012).

729 55. B. K. McColl, S. A. Stacker, M. G. Achen, Molecular regulation of the VEGF family - Inducers of
730 angiogenesis and lymphangiogenesis, *Apmis* **112**, 463–480 (2004).

731 56. S. Lee, T. T. Chen, C. L. Barber, M. C. Jordan, J. Murdock, S. Desai, N. Ferrara, A. Nagy, K. P.
732 Roos, M. L. Iruela-Arispe, Autocrine VEGF Signaling Is Required for Vascular Homeostasis, *Cell* **130**,
733 691–703 (2007).

734 57. J. Siedlecki, C. Wertheimer, A. Wolf, R. Liegl, C. Priglinger, S. Priglinger, K. Eibl-Lindner,
735 Combined VEGF and PDGF inhibition for neovascular AMD: anti-angiogenic properties of axitinib on
736 human endothelial cells and pericytes *in vitro*, *Graefe's Arch. Clin. Exp. Ophthalmol.* **255**, 963–972
737 (2017).

738 58. N. Yamamoto, T. Oyaizu, M. Enomoto, M. Horie, M. Yuasa, A. Okawa, K. Yagishita, VEGF and
739 bFGF induction by nitric oxide is associated with hyperbaric oxygen-induced angiogenesis and muscle
740 regeneration, *Sci. Rep.* **10**, 2744 (2020).

741 59. R. Hlushchuk, M. Ehrbar, P. Reichmuth, N. Heinimann, B. Styp-Rekowska, R. Escher, O. Baum, P.

742 Lienemann, A. Makanya, E. Keshet, V. Djonov, Decrease in VEGF expression induces intussusceptive
743 vascular pruning, *Arterioscler. Thromb. Vasc. Biol.* **31**, 2836–2844 (2011).
744 60. D. R. Murdoch, R. G. Corey, B. Hoen, M. Miró, V. G. Fowler, A. S. Bayer, A. W. Karchmer, L.
745 Olaison, P. A. Pappas, P. Moreillon, S. T. Chambers, V. H. Chu, V. Falcó, D. J. Holland, P. Jones, J. L.
746 Klein, N. J. Raymond, K. M. Read, M. F. Tripodi, R. Utili, A. Wang, C. W. Woods, C. H. Cabell,
747 Clinical presentation, etiology, and outcome of infective endocarditis in the 21st century The
748 international collaboration on Endocarditis-prospective cohort study, *Arch. Intern. Med.* **169**, 463–473
749 (2009).
750 61. J. W. Shupp, M. Jett, C. H. Pontzer, Identification of a transcytosis epitope on staphylococcal
751 enterotoxins, *Infect. Immun.* **70**, 2178–2186 (2002).
752 62. B. A. Fields, E. L. Malchiodi, H. Li, X. Ysern, C. V Stauffacher, P. M. Schlievert, K. Karjalainen, R.
753 A. Mariuzza, Crystal structure of a T-cell receptor β-chain complexed with a superantigen, *Nature* **384**,
754 188–192 (1996).
755 63. L. Leder, A. Llera, P. M. Lavoie, M. I. Lebedeva, H. Li, R. P. Sékaly, G. A. Bohach, P. J. Gahr, P.
756 M. Schlievert, K. Karjalainen, R. A. Mariuzza, A mutational analysis of the binding of staphylococcal
757 enterotoxins B and C3 to the T cell receptor beta chain and major histocompatibility complex class II, *J.*
758 *Exp. Med.* **187**, 823–833 (1998).
759 64. R. Ulrich, S. Bavari, M. Olson, Staphylococcal enterotoxins A and B share a common structural
760 motif for binding class II major histocompatibility complex molecules, *Nat. Struct. Biol.* **2**, 554–560
761 (1995).
762 65. J. W. Kappler, A. Herman, J. Clements, P. Marrack, Mutations defining functional regions of the
763 superantigen staphylococcal enterotoxin B, *J. Exp. Med.* **175**, 387–396 (1992).
764 66. N. W. M. de Jong, T. van der Horst, J. A. G. van Strijp, R. Nijland, Fluorescent reporters for
765 markerless genomic integration in *Staphylococcus aureus*, *Sci. Rep.* **7**, 43889 (2017).
766 67. D. G. Gibson, L. Young, R.-Y. Chuang, J. C. Venter, C. A. Hutchison III, H. O. Smith, Enzymatic
767 assembly of DNA molecules up to several hundred kilobases, *Nat. Methods* **6**, 343 (2009).

768 68. M. R. Grosser, A. R. Richardson, in *Methods in Molecular Biology*, J. L. Bose, Ed. (Springer New
769 York, New York, NY, 2016), vol. 1373, pp. 51–57.
770 69. J. A. Merriman, P. M. Schlievert, in *Methods in Molecular Biology*, A. J. Brosnahan, Ed. (Springer
771 New York, New York, NY, 2016), vol. 1396, pp. 19–33.
772 70. K. N. Gibson-Corley, A. K. Olivier, D. K. Meyerholz, Principles for Valid Histopathologic Scoring
773 in Research, *Vet. Pathol.* **50**, 1007–1015 (2013).
774 71. W.-H. Zhu, R. F. Nicosia, The thin prep rat aortic ring assay: A modified method for the
775 characterization of angiogenesis in whole mounts, *Angiogenesis* **5**, 81–86 (2002).
776 72. J. Stiffey-Wilusz, J. A. Boice, J. Ronan, A. M. Fletcher, M. S. Anderson, An ex vivo angiogenesis
777 assay utilizing commercial porcine carotid artery: Modification of the rat aortic ring assay, *Angiogenesis*
778 **4**, 3–9 (2001).
779 73. J. M. King, K. Kulhankova, C. S. Stach, B. G. Vu, W. Salgado-Pabón, Phenotypes and Virulence
780 among *Staphylococcus aureus* USA100, USA200, USA300, USA400, and USA600 Clonal Lineages ,
781 *mSphere* **1**, e00071-16 (2016).
782
783 **Acknowledgements:** We thank the University of Iowa Comparative Pathology Laboratory and
784 University of Iowa Diagnostic Laboratories for histology and serum analysis services. **Funding:** This
785 work was supported by National Institutes of Health (NIH) grant R01AI34692-01 to W.S-P**,** NIH grant
786 5T32AI007511-23 to P.M.T., and NIH grant T32GM008365 to K.J.K. **Author Contributions:** K.J.K.,
787 S.S.T., J.E.G. and W.S-P conceptualized and designed experiments, analyzed the data, and wrote the
788 manuscript. K.J.K, P.M.T, A.N.F, K.K, and W.S-P carried out *in vivo* rabbit experiments. K.N.G-C
789 provided intellectual and technical support on histopathological analysis and gross pathological grading.
790 S.S.T. carried out ex vivo experiments. X-J. W carried out qPCR analyses. N.S.B. carried out T cell
791 proliferation assays, analyzed the data. All authors reviewed the manuscript. **Competing Interests:**
792 K.J.K. is currently an employee of Integrated DNA Technologies, which sells reagents used or like those

used in this manuscript. **Data and materials availability:** All the data needed to evaluate the conclusions in this manuscript are present in the manuscript and/or supplementary materials.

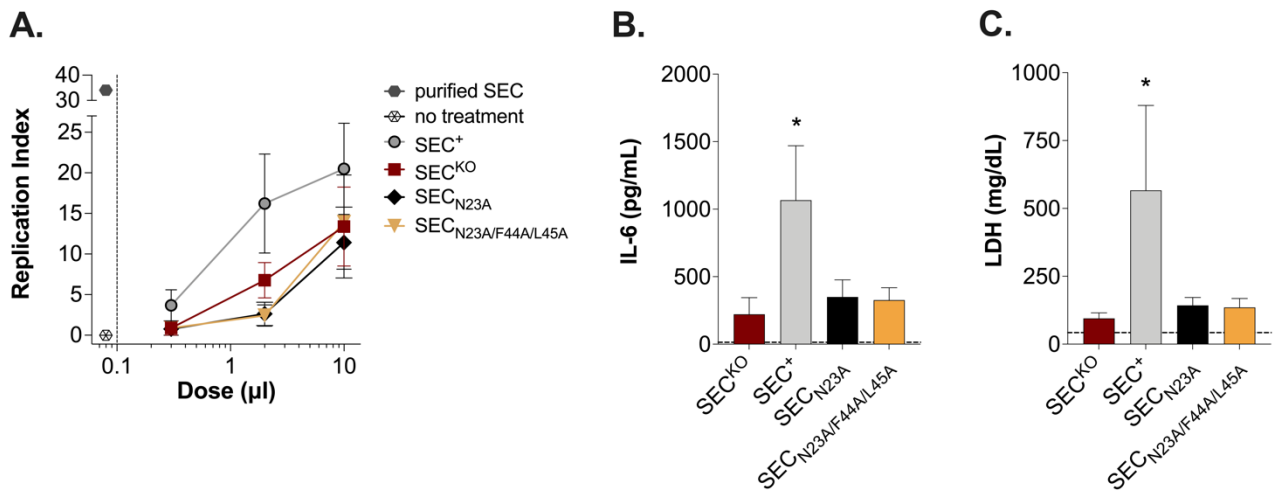

Figure 1. SEC toxoids are deficient in superantigen activity. (**A**) $CD4^+$ T cell replication index of peripheral blood mononuclear cells (PBMCs) stimulated for 6 days with 0.3, 2, and 10 µl of cell-free supernates from overnight cultures of *S. aureus* SEC^{KO}, SEC^+, SEC_{N23A}, and $SEC_{N23A/F44A/L45A}$. PBMCs ± 10 µg of purified SEC were used as controls. (**B-C**) Serum levels of interleukin-6 (IL-6) and lactate dehydrogenase (LDH) 48-96 h post-infection with indicated *S. aureus* strains in experimental infective endocarditis. *S. aureus* SEC^+ (n=12), *S. aureus* SEC^{KO} (n=15), *S. aureus* SEC_{N23A} (n=17), and *S. aureus* $SEC_{N23A/F44A/L45A}$ (n=17). Data are represented as mean (± SEM). The dashed line is the average analyte value of all rabbits pre-infection. Statistical significance was determined by one-way ANOVA with Holm-Šídák's multiple comparisons test with each SEC-producing strain compared to *S. aureus* SEC^{KO}. All experimental groups were tested against pre-infection values and were statistically significant, $p < 0.0001$. (**B**) *, $p = 0.03$. (**C**) *, $p = 0.02$.

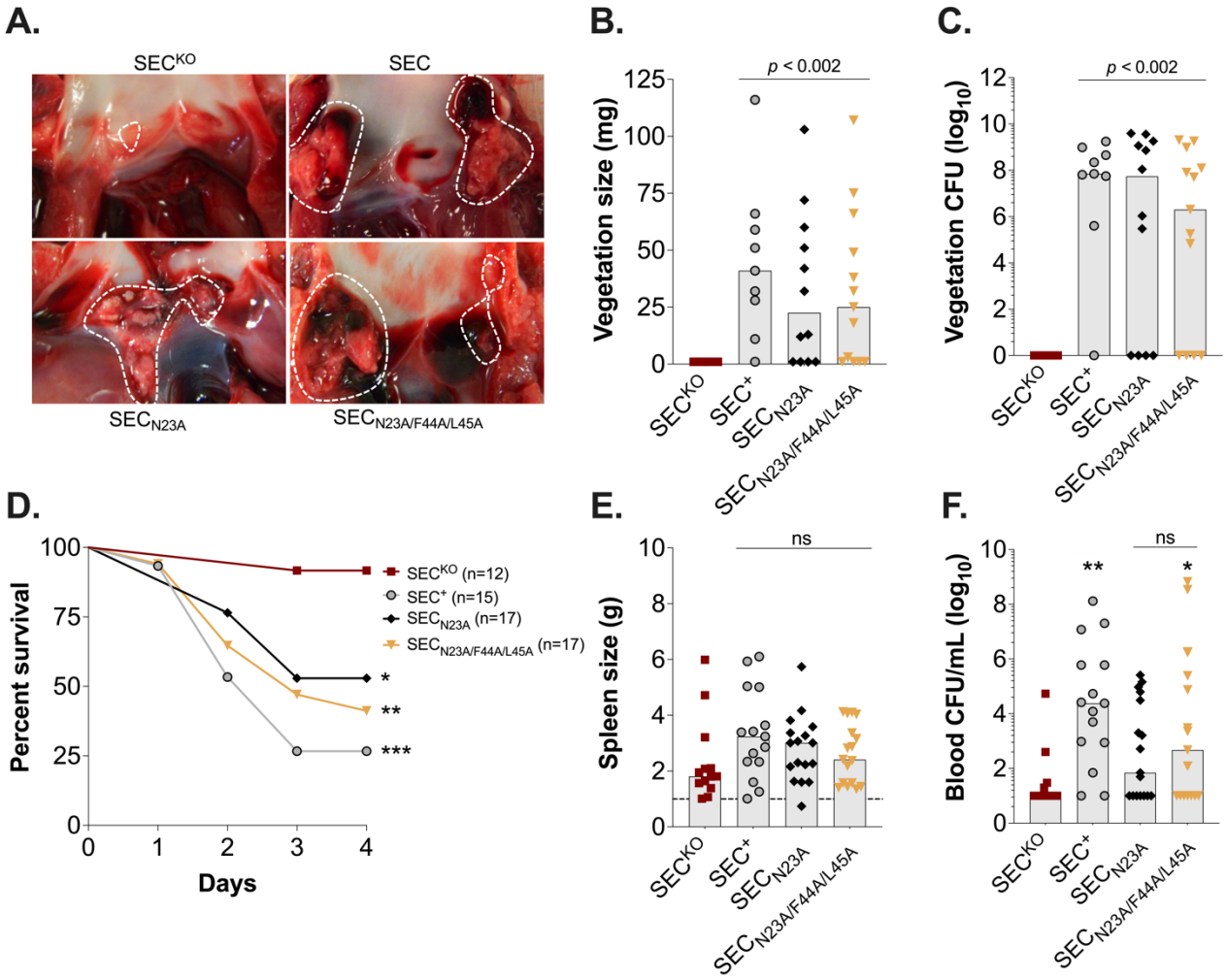

Figure 2. SEC is required for vegetation formation independent of superantigenic activity in the rabbit model of native valve infective endocarditis and sepsis. (**A**). Representative images of aortic vegetations (areas indicated with dash-lines). (**B**) Total weights of vegetations dissected from aortic valves from infected rabbits. (**C**) Bacterial counts recovered from aortic vegetations. (**A-C**) Bars represent median value. Statistical significance, one-way ANOVA with Holm-Šídák's multiple comparisons test compared to SEC^{KO}. (**D**) Percent survival of rabbits infected intravenously with $2x10^7$–$4x10^7$ CFU of indicated strain over 4 days. *, $p = 0.03$, **, $p = 0.006$, ***, $p = 0.0007$ log-rank Mantel-Cox Test. (**E**) Enlargement of the spleen resulting from *S. aureus* infection. (Dashed line) Average spleen size of uninfected rabbit controls (0.86 ± 0.1, n = 3). (**F**) Bacterial counts per milliliter of blood recovered from rabbits *post-mortem*. (**D-F**) Bars represent median value. *, $p = 0.03$, **, $p = 0.003$, ns = not significant, one-way ANOVA with Holm-Šídák's multiple comparisons test. Statistical significance compared to SEC^{KO}.

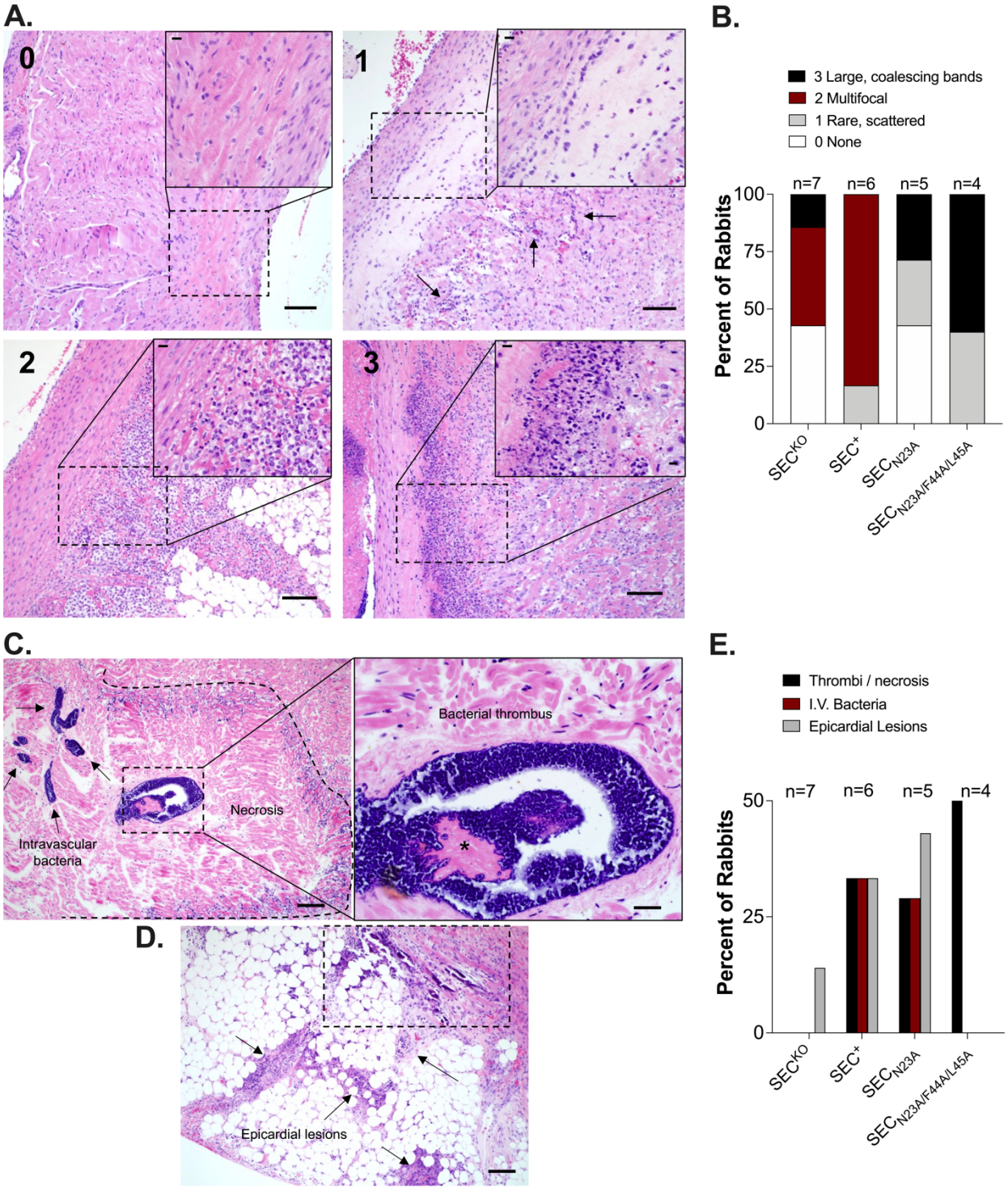
A.
0
1
2
3
B.
3 Large, coalescing bands
2 Multifocal
1 Rare, scattered
0 None
n=7
n=6
n=5
n=4
Percent of Rabbits
100
75
50
25
0
SEC^KO
SEC^+
SEC_N23A
SEC_N23A/F44A/L45A
C.
Bacterial thrombus
Necrosis
Intravascular bacteria
*
D.
Epicardial lesions
E.
Thrombi / necrosis
I.V. Bacteria
Epicardial Lesions
n=7
n=6
n=5
n=4
Percent of Rabbits
50
25
0
SEC^KO
SEC^+
SEC_N23A
SEC_N23A/F44A/L45A

Figure 3. Vegetative lesions present with bacterial infiltration, inflammation, and necrosis. (**A**) Examples of histopathologic assessment of myocardial inflammation during rabbit model of native valves infective endocarditis (Graded 0-3). Inflammation was graded based on the amount of inflammatory cell infiltrate noted within the myocardium. 0 = no inflammation, 1 = rare, scattered infiltrate (arrows), 2 = multifocal bands of infiltrate, 3 = large, coalescing bands of diffuse infiltrate with necrosis. Bar = 100 µm, inset bar = 20 µm. (**B**) Scoring of myocardial inflammation from H&E-stained images 48 – 96 h post-infection. No statistical significance among wildtype and toxoid groups, Fisher's exact test with categorical pathology grades 0-1 and grades 2-3 against SEC^{KO}. (**C**) Examples of a fibrinonecrotic focus (dotted outline; note the myocardial necrosis within the outline which is a lighter pink color), (*) a centrally located septic thrombus, and (arrows) intravascular bacteria (deeply basophilic/blue material). Left bar = 100 µm, right bar = 20 µm. (**D**) Examples of an epicardial lesion with saponification (necrosis) of epicardial fat (arrows) and a locally extensive zone of myocardial mineralization (dotted rectangle). Bar = 100 µm. (**E**) Histopathology scoring for the presence or absence of cardiac pathological findings: bacterial thrombi and associated necrosis, intravascular (IV) bacteria, and epicardial fibrin and inflammation.

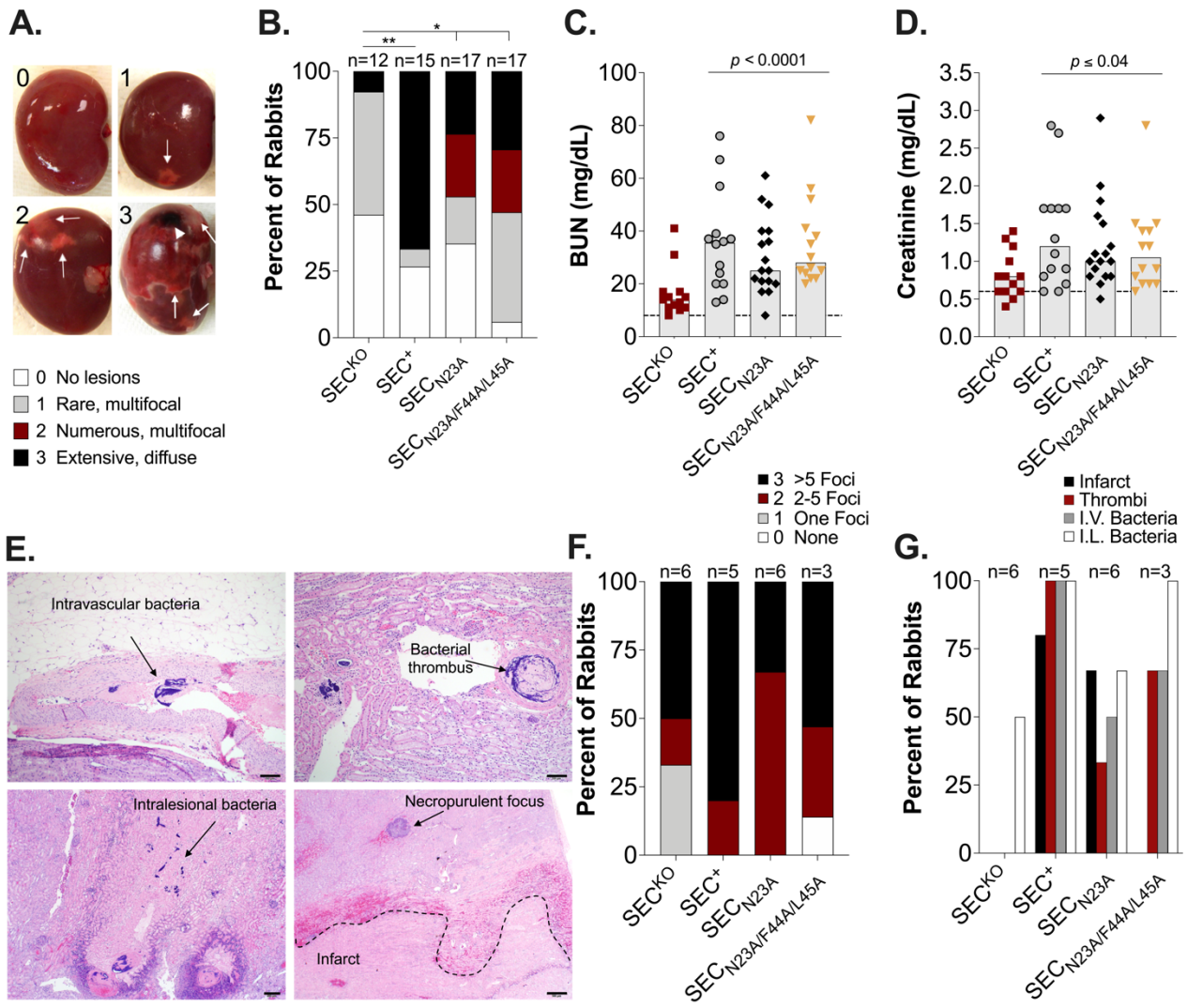

Figure 4. SEC toxoids retain the ability to cause metastatic infections and acute kidney injury. (**A**) Kidney Gross Pathology Grading Scale during rabbit model of native valves infective endocarditis (Grades 0-3). 0 = no lesions, 1 = rare, small (<4mm) multifocal lesions, 2 = numerous large (>5mm) multifocal lesions, 3 = extensive to coalescing to diffuse lesions. Arrows indicate ischemic and/or hemorrhagic lesions, arrowhead indicates a necrotic lesion. (**B**) Scoring of kidney lesions *post-mortem*. *, $p \leq 0.0432$, **, $p = 0.0047$, Fisher's exact test between categorical pathology grades 0-1 and grades 2-3 against SEC^{KO}. (**C-D**) Serum levels of analytes 48 – 96 h post-infection. Bars represent median value. Dashed line is the average analyte value of all rabbits pre-infection. All groups were tested against pre-infection analyte values and were statistically significant, $p < 0.03$, one-way ANOVA with Holm-Šídák's multiple comparisons test. (**E**) Examples of histopathologic assessment for the presence or absence of intravascular bacteria (top-left panel, arrow), bacterial thrombi (top-right panel, arrow), intralesional bacteria (bottom-left panel, arrow), and infarcts (bottom-right panel, area below dash

line). Bar = 100 µm (top-left and right panels). Bar = 200 µm (bottom-left panel). Bar = 500 µm (bottom-right panel). (**F**) Histopathologic scoring of smaller foci of necropurulent inflammation (Graded 0-3) as shown in **E**, bottom-right panel. 0 = none, 1 = one foci, 2 = 2-5 foci, 3 $\geq$ 5 foci. (**G**) Histopathologic scoring for the presence or absence of kidney lesions, as shown in **E**: Ischemic necrosis (infarct), bacterial thrombi, intravascular (I.V.) bacteria, and intralesional (I.L.) bacteria.

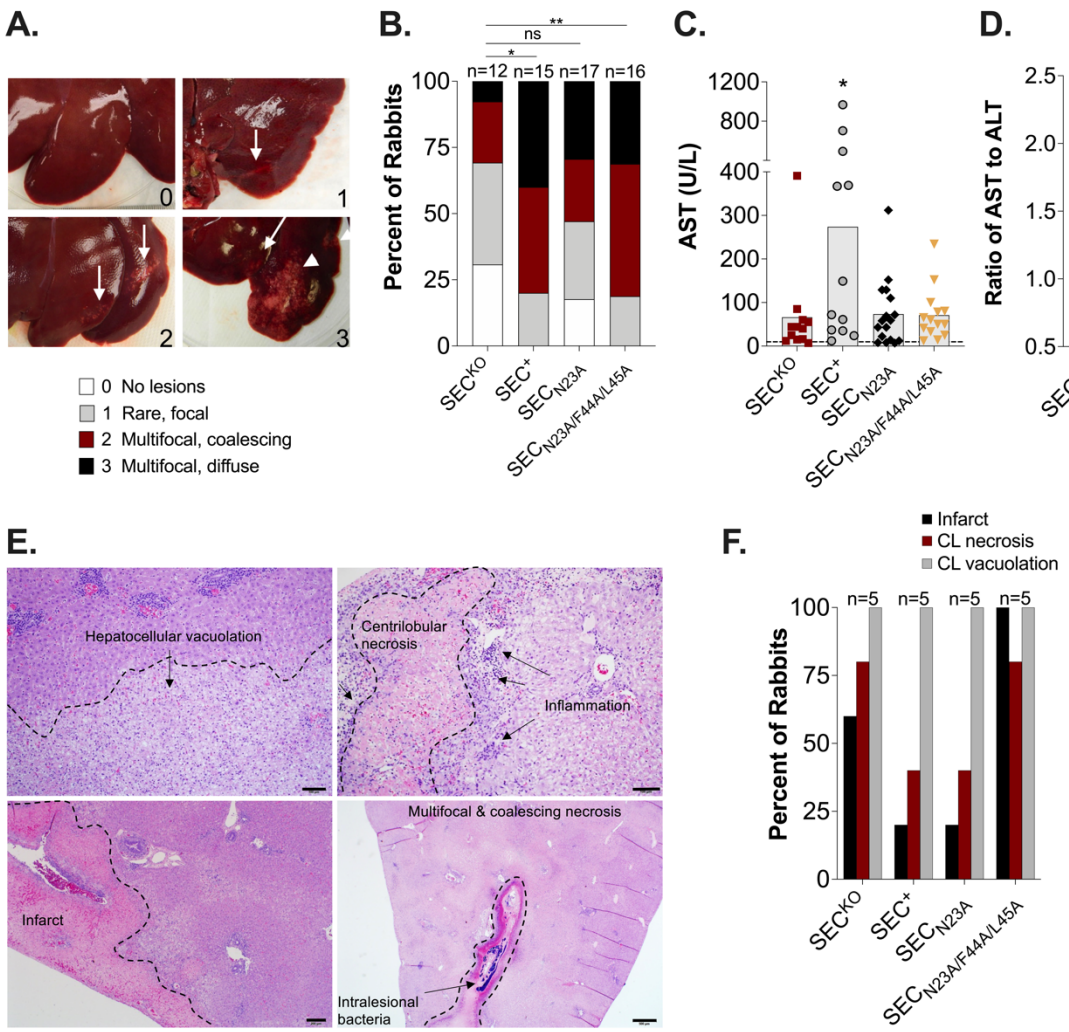

Figure 5. Superantigenicity promotes hepatocellular injury. (**A**) Liver gross pathology grading scale during rabbit model of native valves infective endocarditis (Grades 0-3). 0 = no lesions, 1 = rare, focal streak-shaped lesions, 2 = multifocal to coalescing streak-shaped lesions, 3 = multifocal streak-shaped, extensive to diffuse lesions. Arrows point to streak-shaped ischemic lesions characteristic of grade 1-3, arrowhead indicate wide-spread ischemic lesions characteristic of grade 3. (**B**) Scoring of liver pathology *post-mortem*. *, $p = 0.02$, **, $p = 0.009$, Fisher's exact test between categorical pathology grades 0-1 and grades 2-3 against SEC^{KO}. (**C-D**) Serum levels of analytes 48 – 96 h post infection. Dashed line is the average analyte or ratio value of all rabbits pre-infection. (**C**) Bars represent median value. *, $p \leq 0.01$, one-way ANOVA with the Holm-Šídák's multiple comparisons test; *S. aureus* SEC^{KO} compared to other strains. All groups were tested against pre-infection AST values and were statistically significant, $p < 0.005$. (**D**) Data are represented as mean (± SEM). *, $p \leq 0.01$, Fisher's exact test comparing ratio values 0-1.8 to values > 1.8 between *S. aureus* SEC^{+} and the rest of the experimental groups. (**E**) Examples of liver lesions observed upon histopathologic assessment. (Top-left panel) locally extensive hepatocellular vacuolation with arrow showing area under dashed line with cytoplasmic vacuolation. (Top-right panel) diffuse centrilobular necrosis (area inside dashed line), surrounded by necropurulent inflammation (arrows). (Bottom-left

panel) large zone of necrosis (infarction), area left of the dash line, with multifocal to coalescing portal hepatocellular vacuolation shown on region right of the dash line (arrows show examples). Bar = 100 µm (top-left and right panels). Bar = 200 µm (bottom-left panel). Bar = 500 µm (bottom-right panel). (**F**) Histopathologic scoring for the presence or absence infarcts, centrilobular (CL) necrosis, and centrilobular (CL) vacuolation.

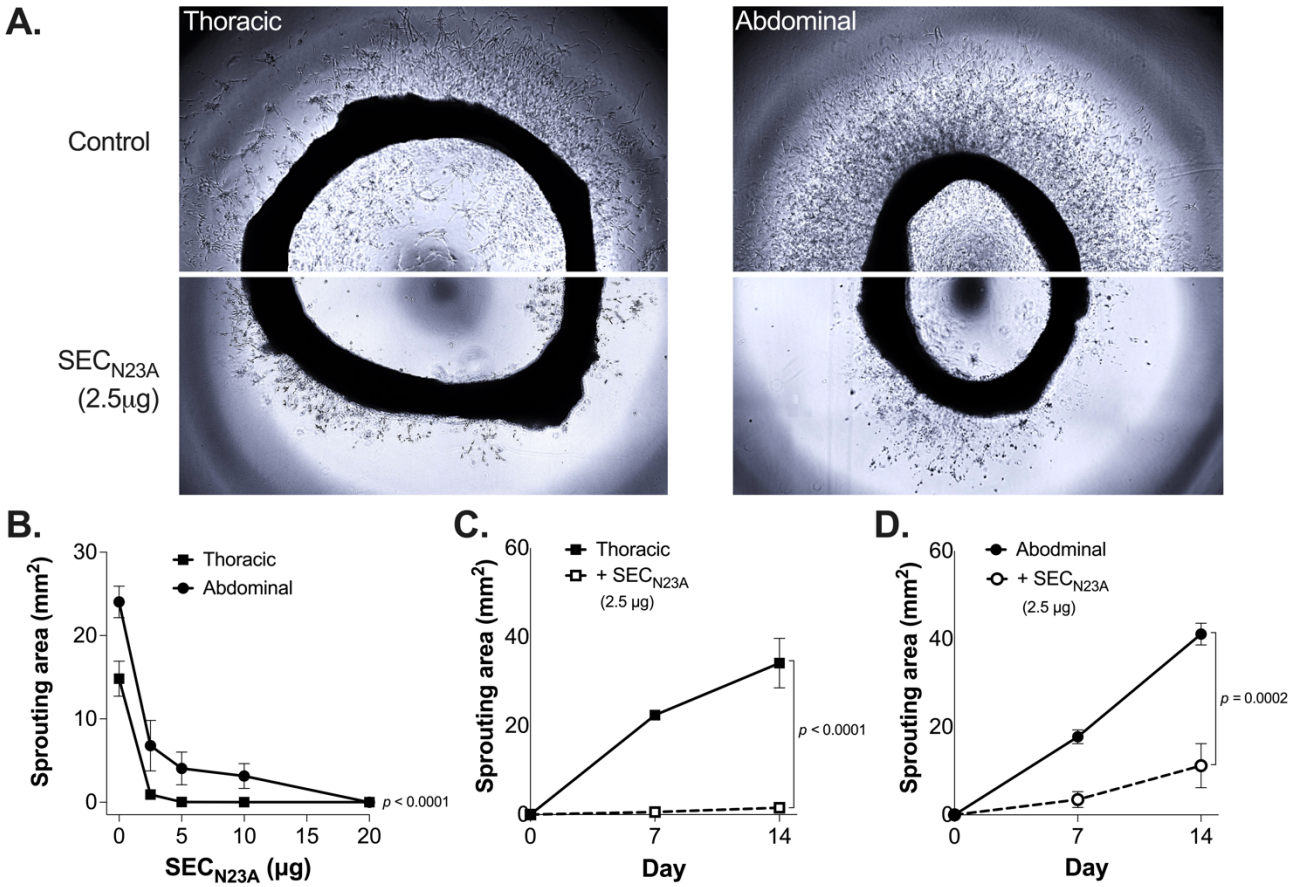

Figure 6. SEC suppresses sprouting of new capillaries in the *ex vivo* rabbit aortic ring model of angiogenesis. Thoracic and abdominal aortic ring explants were cultured in the presence of SEC_{N23A} for 14 days. (**A**) Aortic rings imaged at day 14 showing capillary network formation sprouting from the rings in culture conditions (top panels) versus treatment with 2.5 µg of SEC_{N23A} (bottom panels). (**B**) Quantification of sprouting area (mm^2) in aortic rings treated with 2.5, 5, 10, 15, and 20 µg of SEC_{N23A} for 14 days. (**C**) Time course analysis of thoracic aortic ring sprouting in the presence (solid squares) or absence (empty squares) of 2.5 µg of SEC_{N23A}. (**D**) Time course analysis of abdominal aortic ring sprouting in the presence (solid circles) or absence (empty circles) of 2.5 µg of SEC_{N23A}. (**B-D**) Statistical significance was determined by two-way ANOVA with the Holm-Šídák's multiple comparisons test. P values denote significance between treatment and no-treatment conditions.

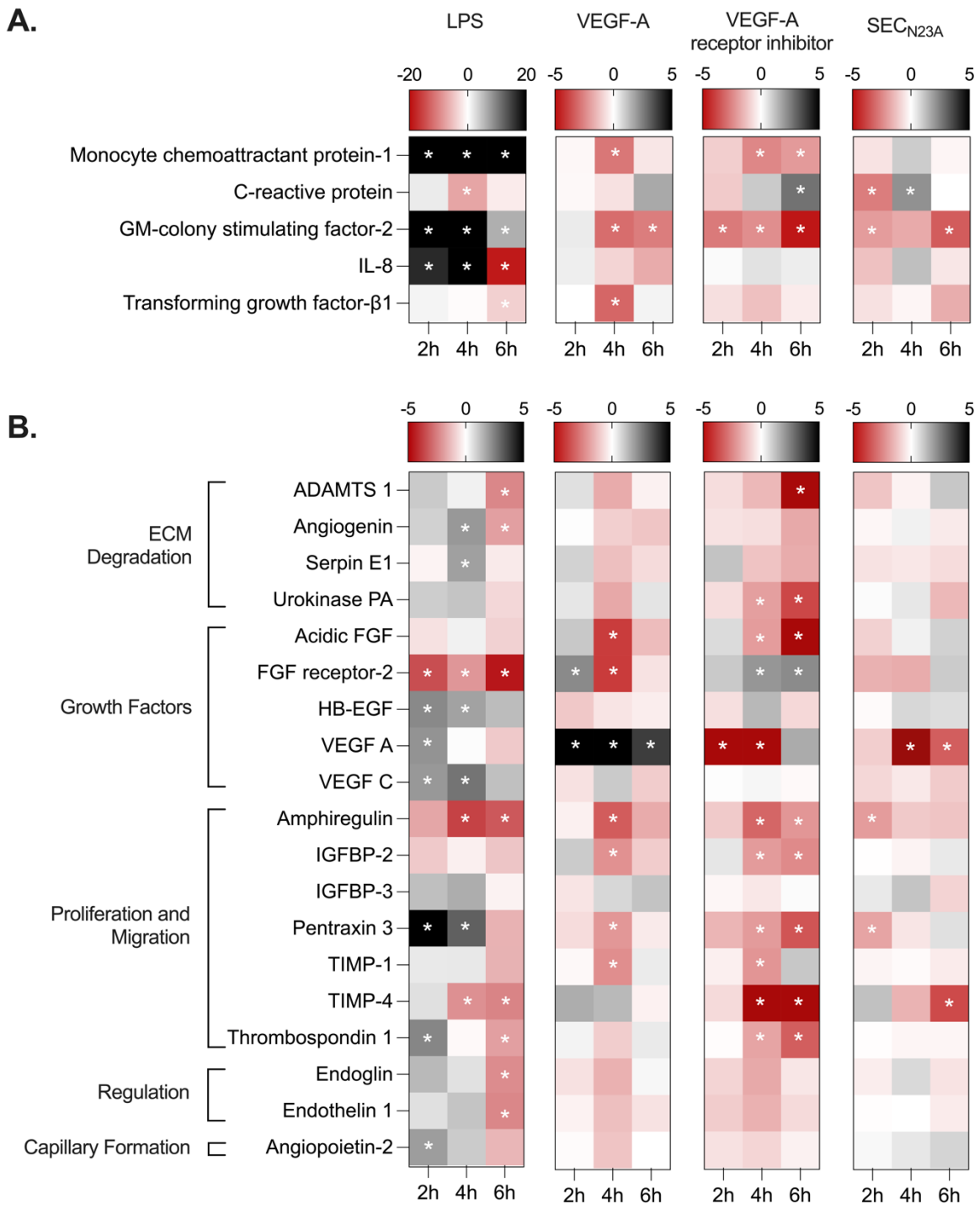

Figure 7. SEC inhibits VEGF-A expression in immortalized human aortic endothelial cells. Expression analysis of 24 angiogenesis-related genes by RT-qPCR in iHAECs treated with lipopolysaccharide (LPS, 25 ng mL^{-1}), VEGF-A (20 nM), VEGF-A receptor inhibitor (axitinib, 25 nM), or SEC_{N23A} (20 µg mL^{-1}) for 2, 4, and 6 h. (**A**) Gene products that play significant roles in inflammatory responses. (**B**) Gene products that contribute to various angiogenesis processes. *, denotes genes with 2-fold increases or decreases compared to untreated controls.

Supplementary materials and methods

SDS-PAGE and quantitative western blotting

S. aureus strains were grown for 24 h in TH. 5 mL of culture was precipitated in 20 ml of 100% EtOH (Final Concentration 80% EtOH) and stored at 4°C overnight. Precipitates were collected by centrifugation at 4°C for 10 min at 1000 x g. Supernatants were poured off and precipitates were allowed to dry, resuspended in 250 µl of PBS, and centrifuged at room temperature for 10 min at 21,000 x g. The supernatants were collected and total protein quantified by Bradford assay according to manufacturer's instructions using bovine serum albumin as a standard (Bio-Rad Laboratories). Samples were normalized to a protein concentration of 0.4 mL^{-1}, diluted 1:20 in PBS, mixed with 2X sample buffer, boiled for 5 min, and electrophoresed along with purified SEC as a standard curve on a 12% Mini-PROTEAN® TGX Stain-Free™ gel (Bio-Rad Laboratories) at 200V for 40 min. Samples were transferred to an Immobilon-FL polyvinylidene fluoride (PVDF) membrane (MilliporeSigma) by electroblotting at 100V, 250mA for 90 min at 4°C in Towbin Buffer with 20% EtOH substituted for methanol. Membranes were blocked for 1 h at room temperature with 10% nonfat dry milk and 5% heat inactivated horse serum (Gibco Life Technologies) in PBS and then incubated overnight at 4°C with rabbit polyclonal anti-SEC antibody (1:10,000) in 5% nonfat dry milk and 2.5% heat inactivated horse serum in PBS. The membrane was washed with PBST (PBS with 0.1% Tween 20) and incubated with goat anti-rabbit antibody IRDye 800CW (LI-COR, 1:20,000) for 1 h at room temperature. Blots were washed with PBST and visualized using an Odyssey CLx (169 µm resolution, auto intensity 800 nm channel) and analyzed with Image Studio software (LI-COR). SEC production was quantified by standard curve method using purified SEC and densitometrical analysis. Data is represented from 5 independent experiments with technical triplicates.

S. aureus growth curves

Overnight cultures were diluted to an OD_{600} 1.0 in TH. 10 µl of diluted culture was added to 190 µl of TH in a 96-well round, clear bottom plate in technical triplicate (Corning). Plates were sealed using Breathe-Easy sealing membrane (Diversified Biotech). Growth was measured using a TECAN M200 plate reader overnight with the following settings: 37°C, 30 min kinetic interval, orbital shaking: amplitude 3 mm for 10 s before reads, 1 read/well at 600 nM, 25 flashes, 9 nM bandwidth, 100ms settle time, and 27 min wait time between reads with orbital shaking: amplitude 3mm for 26.5 min. Data is represented by three independent experiments.

Erythrocyte lysis assays for hemolysin production

Erythrocyte Lysis assays were performed as previously described *(73)*. Overnight cultures were diluted to an OD_{600} 1.0 in PBS and 5 µl spotted onto TSA II agar plates with either 5% rabbit or sheep blood (Becton Dickinson). Plates were incubated for 24 h at 37°C with 5% CO_2. Zones of hemolysis were measured and quantified using ImageJ. Data is represented by three independent experiments done with technical duplicates.

MTS assay

An MTS assay was used to determine cell viability. Cells were seeded at 7,000 cells/well into gelatin-coated 96-well plates and grown overnight to near confluency. Media was removed and replaced with 100 µL of media containing increasing concentrations of SEC or SEC_{N23A} at 20 µg mL^{-1} followed by overnight incubation. 20 µL of CellTiter 96® AQueous One Solution was added to each well followed by a 1 h incubation at 37°C, 5% CO_2. A plate reader was used to read absorbance at 490 nm. Three biological replicates were conducted with each containing three technical replicates. The data were normalized so that untreated cells were considered 100% activity by dividing the absorbance of treated cells by the absorbance of untreated cells.

Supplementary figures

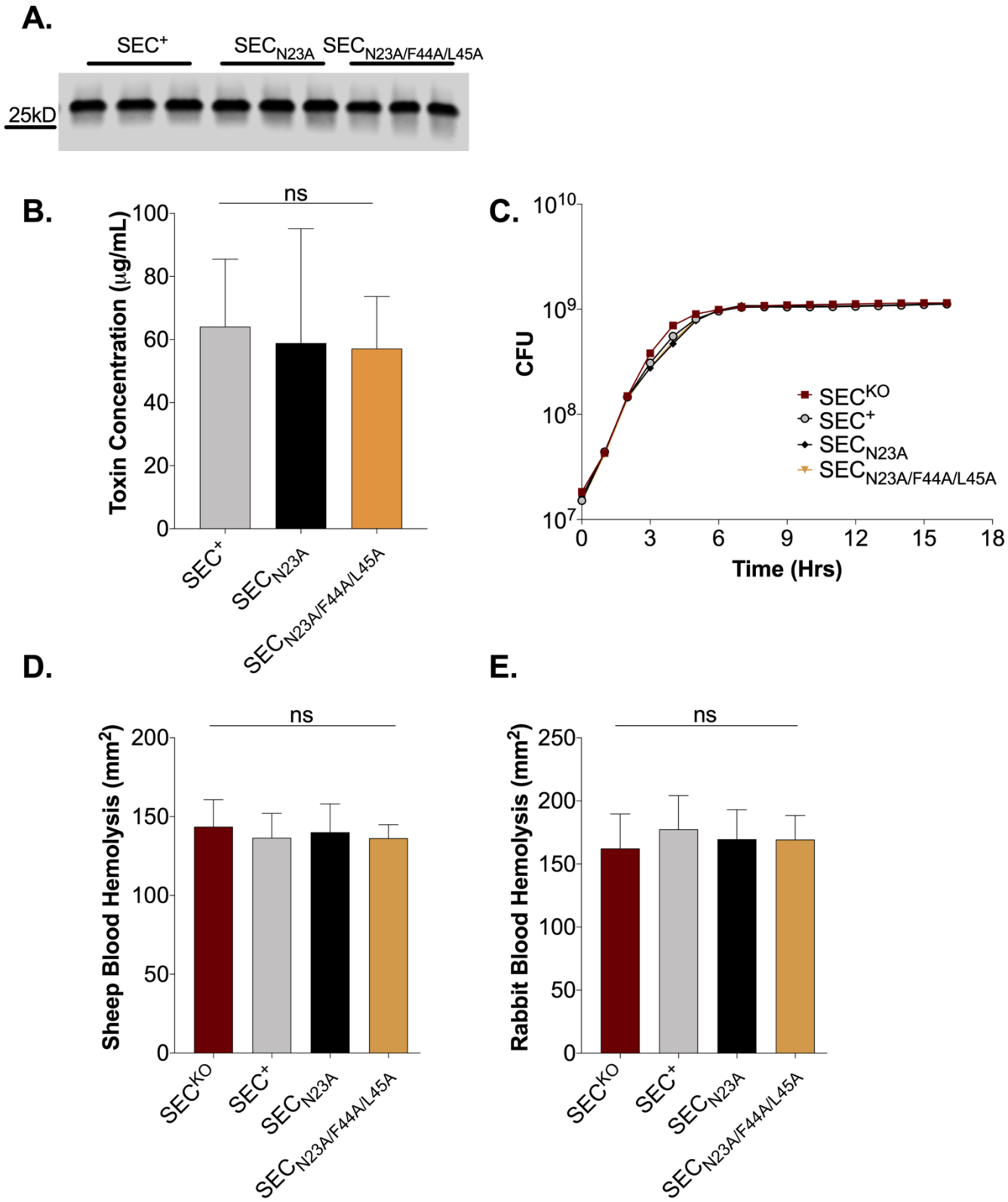

Figure S1. Virulence factor production and growth of strains producing SEC binding site inactivated toxoids. (**A**) Representative western blot images of SEC production in wild-type and SEC complement strains grown overnight in Todd Hewitt (TH) medium shown in technical triplicate. (**B**) Quantitative western blot analysis of SEC production. (**C**) Growth curve of *S. aureus* SEC^{KO}, SEC^{+}, SEC_{N23A}, $SEC_{N23A/F44A/L45A}$ grown overnight in TH. (**D**) Relative levels of hemolysin production as measured in a sheep erythrocyte lysis assay. (**E**) Relative levels of α-hemolysin production as measured in a rabbit erythrocyte lysis assay. (**D, E**) Overnight cultures of *S. aureus* were washed and spotted onto blood agar plates. Zones of hemolysis were measured after overnight growth. Data are represented as mean (± SD). Statistical significance was determined by one-way ANOVA and nonparametric Kruskal-Wallis test. p values ≤ 0.05 are considered statistically significant.

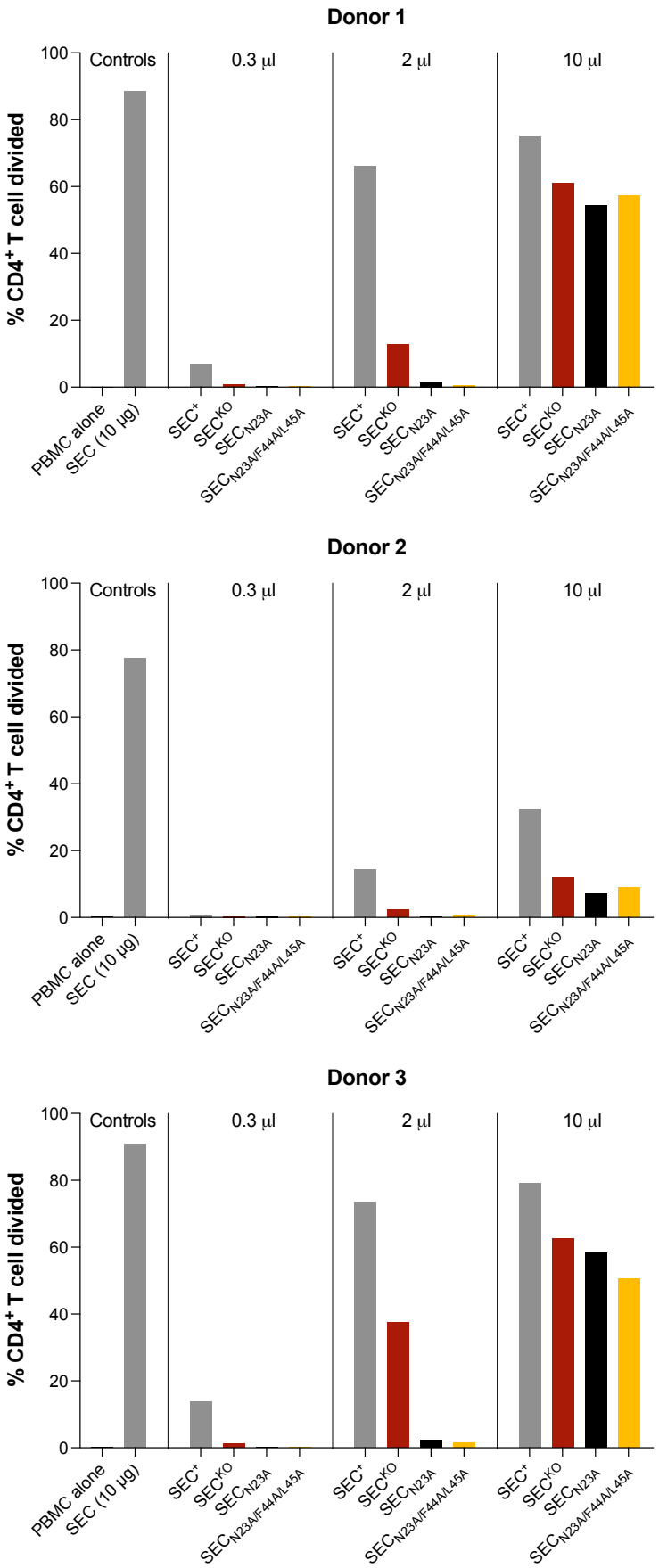
Donor 1
Controls
0.3 µl
2 µl
10 µl
% CD4+ T cell divided
100
80
60
40
20
0
PBMC alone
SEC (10 µg)
SEC+
SECKO
SECN23A
SECN23A/F44A/L45A
Donor 2
Donor 3

Figure S2. SEC toxoids are deficient in superantigen activity. Percent divided of $CD4^+$ T cell from three different human donors. Peripheral blood mononuclear cells (PBMCs) stimulated for 6 days with 0.3, 2, and 10 µl of cell-free supernates from overnight cultures of *S. aureus* SEC^{KO}, SEC^+, SEC_{N23A}, and $SEC_{N23A/F44A/L45A}$. PBMCs ± 10 µg of purified SEC were used as controls.

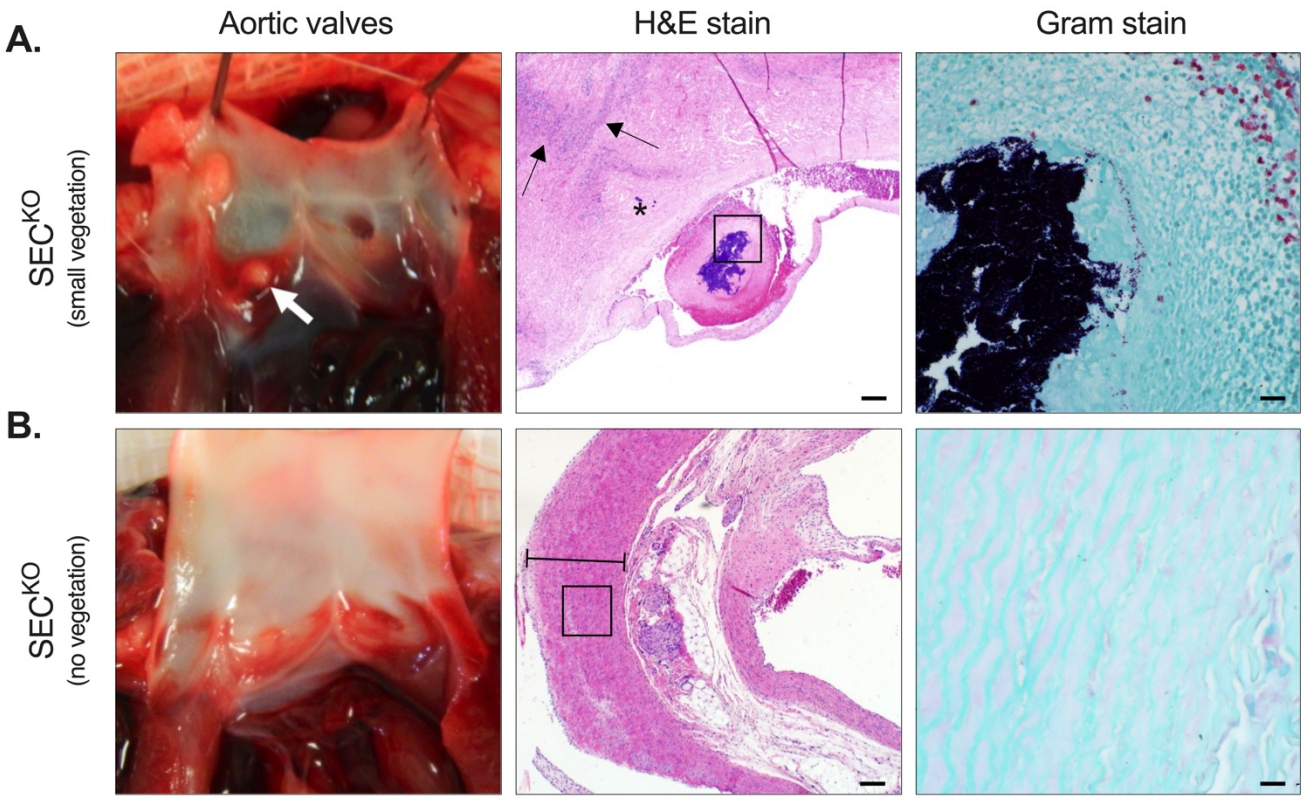

Figure S3. Vegetation formation in rabbits infected with *S. aureus* SEC^{KO}. (**A**) Representative image of the aortic valves from *S. aureus* SEC^{KO} infected rabbits that had small proliferative vegetations (white arrow). H&E stained section of a small vegetation (2.6 mm^2) on the aortic wall with multifocal inflammation throughout the myocardium (arrows) with myocardial infarction adjacent to valvular lesion (star) as well as intralesional bacteria. High magnification Gram stain highlights presence of gram-positive cocci in vegetation. (**B**) Representative image of the aortic valves from *S. aureus* SEC^{KO} infected rabbits that had no proliferative vegetations. H&E stained section of the aortic valve showing no proliferative vegetation, myocardial inflammation, nor visible lesion (perpendicular lines mark the wall of the aorta). High magnification Gram stain image shows absence of bacteria along the myocardium. H&E bar = 200 μm; Gram bar = 20 μm.

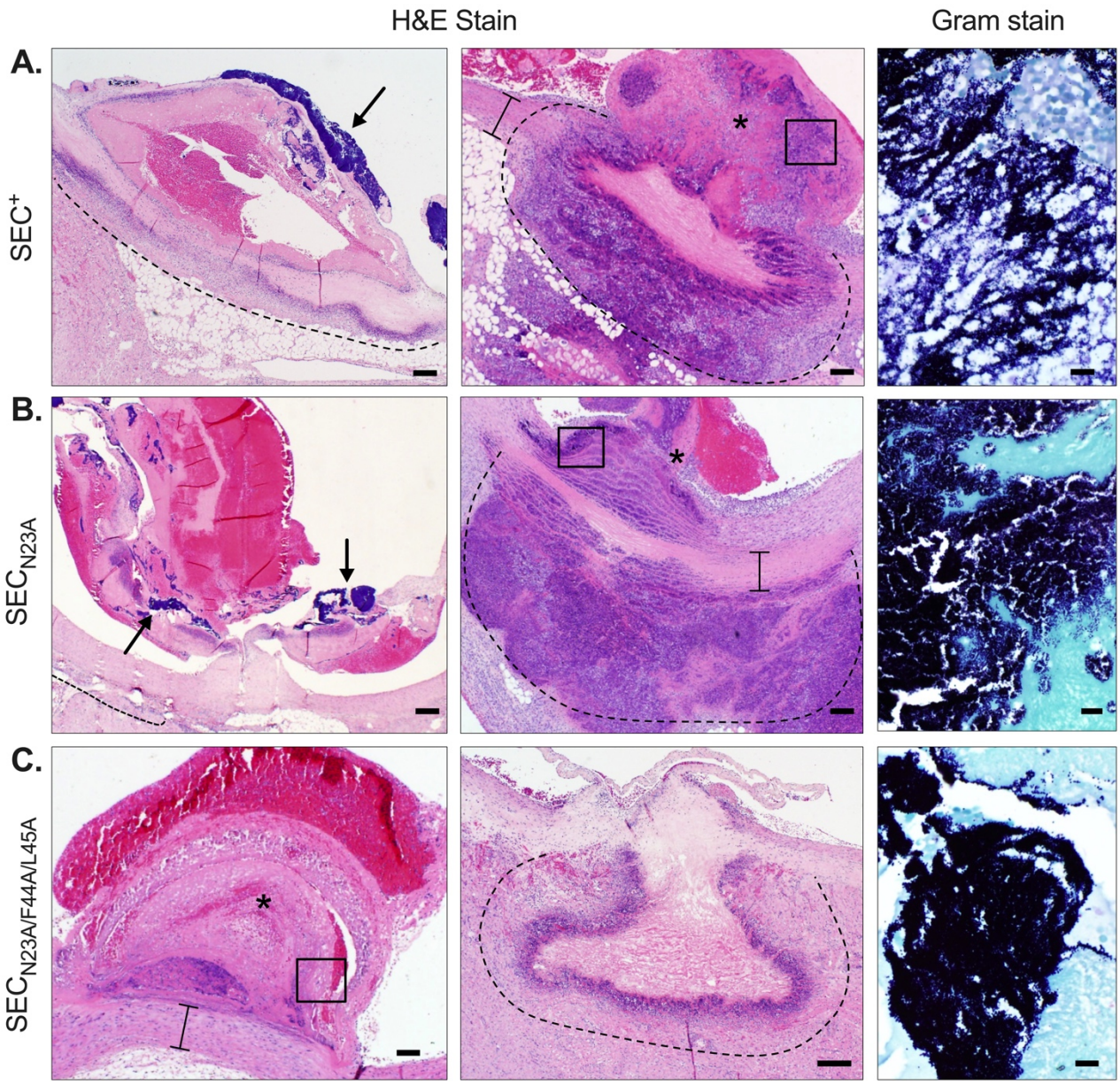

Figure S4. Vegetation formation in rabbits infected with *S. aureus* producing SEC. Images of aortic vegetations from rabbits infected with (**A**) *S. aureus* SEC^+ (4.42 mm^2), (**B**) *S. aureus* SEC_{N23A} (10.5 mm^2), or (**C**) *S. aureus* $SEC_{N23A/F44A/L45A}$ (1.4 mm^2). *Left panels*: H&E stained sections of aortic valve vegetations showing large bacterial clusters on the aortic endothelium (arrows) and a central core of organized fibrin intermixed with erythrocytes, bacterial colonies and debris. (*) marks the proliferative vegetation on **C**. Bands of heterophils adjacent to the myocardium is shown above the dashed lines (**A-B**) and multifocal zones of heterophilic inflammation along the aortic wall (marked with perpendicular lines) is shown in **C**. *Middle panels*: Images of a proliferative vegetations (star) extending transmurally through the aortic wall (perpendicular lines) with large zones of heterophilic inflammation. (**C**) Image shows vessel wall with necrotic cell debris and fibrin with areas of inflammation within the myocardium shown above the dashed lines. *Right panels*: (**D**) High magnification Gram

stain images of a proliferative vegetation from boxed regions in H&E stain showing gram-positive cocci. H&E Bars = 200 μm; Gram bars = 20 μm.

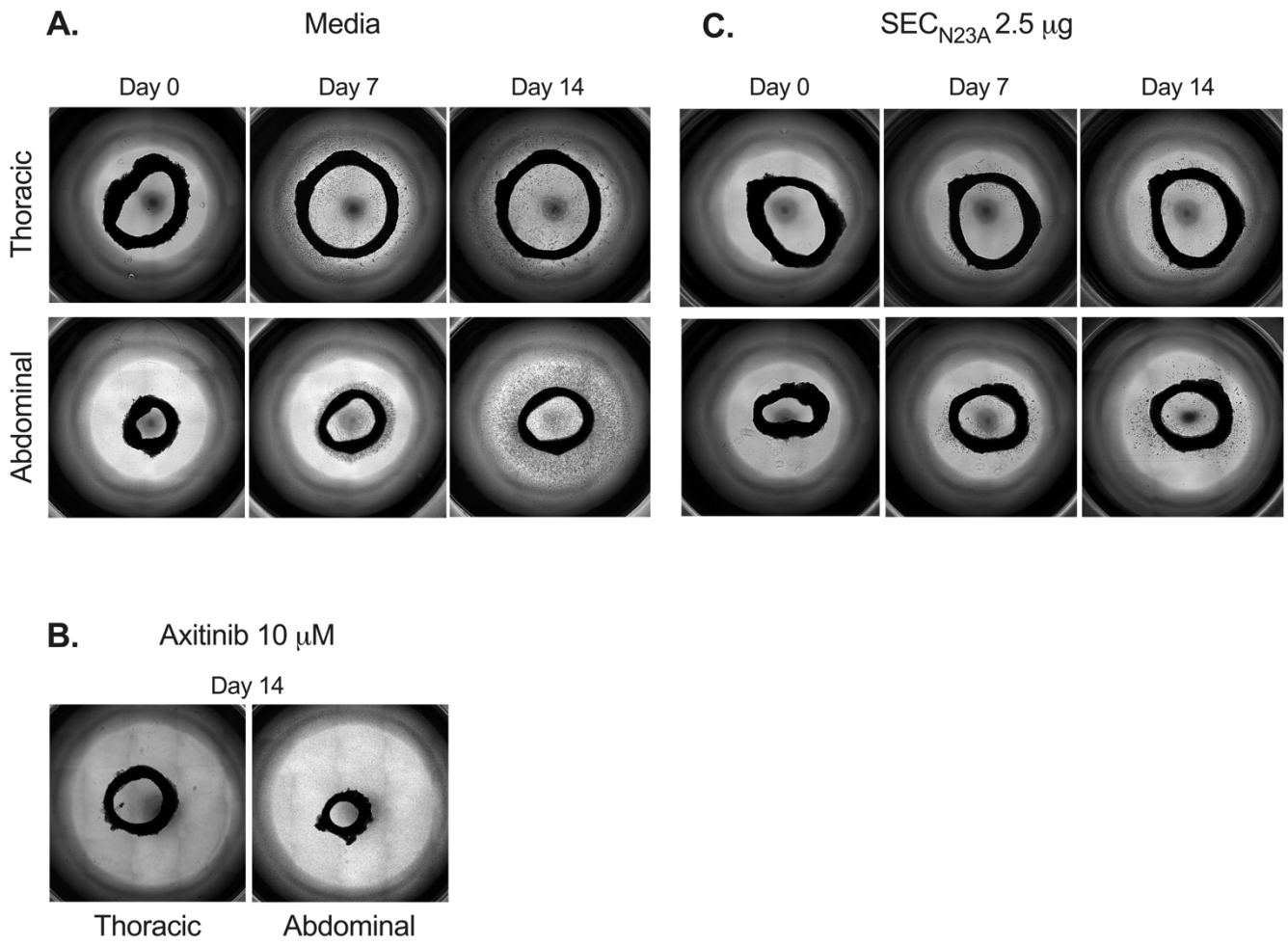

Figure S5. SEC$_{N23A}$ inhibits aortic ring angiogenic sprouting. Thoracic and abdominal aortic ring sections (~1mm wide) derived from 2-3 kg New Zealand white rabbits were embedded in Matrigel basement membrane matrix and cultured in (**A**) media only, (**B**) axitinib (10 μM), or (**C**) SEC$_{N23A}$ (2.5 μg). Sprout formation was captured on day 0, 7, and 14.

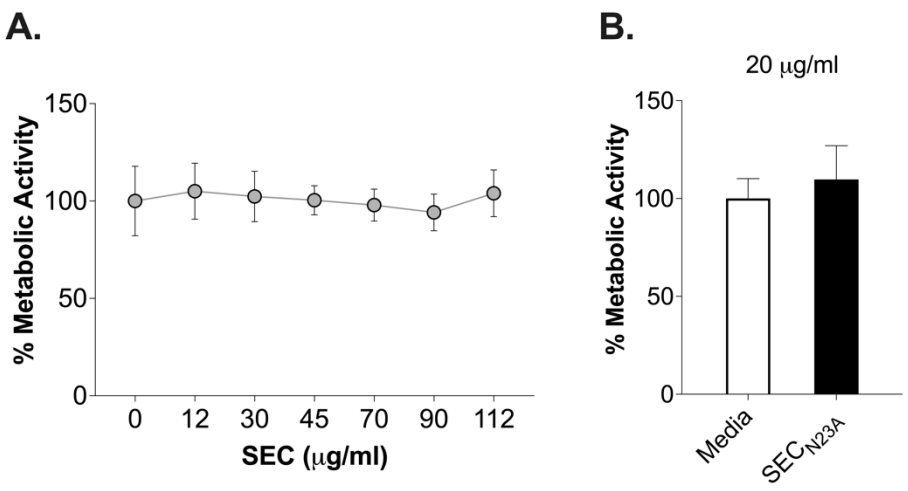

Figure S6. SEC exhibits no cytotoxicity towards immortalized human aortic endothelial cells (iHAECs). Percent metabolic activity of iHAECs grown to near confluency on 1% gelatin-coated plates and treated for 24 h with (**A**) increasing concentrations of SEC (12 – 112 μg mL^{-1}) or (**B**) SEC$_{N23A}$ at the experimental dose (20 μg mL^{-1}). No statistical significance across groups, one-way ANOVA with the Holm-Šídák's multiple comparisons test.

Supplementary Tables

Table S1. Strains and plasmids

Strains	Genotypic Description	Reference
MW2	Wild-type *S. aureus* strain from a pneumonia/TSS clinical isolate	10
MW2Δ*sec*	MW2 with deletion of SEC	10
MW2Δ*sec*::P_{sec}-SEC_{N23A}	Chromosomal complementation of SEC_{N23A} with native MW2 SEC promoter and terminator inserted downstream of MW0058	This Study
MW2Δ*sec*::P_{sec}-$SEC_{N23A/F44A/L45A}$	Chromosomal complementation of $SEC_{N23A/F44A/L45A}$ with native MW2 SEC promoter and terminator inserted downstream of MW0058	This Study
RN4220	Restriction-deficient cloning strain	50
Plasmids		
pJB38-NWMN2930	Temp-sensitive shuttle vector for *S. aureus* markerless chromosomal complementation	46
pUC19	M13 Cloning Vector	51
pKK29	pJB38-NWMN2930 containing SEC_{N23A} with native MW2 SEC promoter and terminator	This Study
pKK33	pUC19 containing SEC_{N23A} with native MW2 SEC promoter and terminator	This Study
pKK39	pUC19 containing $SEC_{N23A/F44A/L45A}$ with native MW2 SEC promoter and terminator	This Study
pKK42	pJB38-NWMN2930 containing $SEC_{N23A/F44A/L45A}$ with native MW2 SEC promoter and terminator	This Study
pET25bHSVdelTEV	pET25b vector with HSV tag deleted and a C-terminal TEV cleavage site inserted upstream of the 6xHis tag	This Study

Table S2. Mutagenesis Primers

Target	Oligo	Sequence 5'-3'
MW2 SEC upstream intergenic region to SEC L27 with N23A mutation in the oligo	pJB38xN23ApromF	GGAGTTTTTTTCTGAGTTAAACGATAACCTGAACCTACTGTTGTTAAAAC
	promN23AR	AAATATTTCATAGCACCCATCGTACCAGTAAAC
MW2 SEC downstream intergenic region to SEC L27 with N23A mutation in the oligo	termN23AF	GGTACGATGGGTGCTATGAAATATTTATATGATGATCATTATG
	pJB38xN23AtermR	TGCAAAATTAAAAATACATCAGGATCAACACAATTTCATCTAGATGTC
SEC_{N23A} with upstream and downstream intergenic regions for insertion into pUC19	pUC19SECN23AptF	TTGTAAAACGACGGCCAGTGAATTCAACCTGAACCTACTGTTGTTAAAAC
	pUC19SECN23AptR	TCTAGAGGATCCCCGGGTACCAACACAATTTCATCTAGATGTC
Mutagenesis primers to insert F44A/L45A mutation into SEC_{N23A}	SECF44A/L45Afor	GATAAAGCAGCAGCACATGATTTAATTTATAACATTAGTGATAAAAAACT
	SECF44A/L45Arev	TAAATCATGTGCTGCTGCTTTATCTACAGACTTAACTTTAGTTGCTGATA
Screening primers for chromosomal insertion	XNWMN2930F	GCTAATGTGATATATGCAACGCC
	XNWMN2930R	GGATGTCCTGTAGCAAATGTTG
Sequencing primers for insertion	pJB38XecoRVF	ATGGTATTTGAGCACGTTTAGCGAC
	pJB38XecoRVR	CACGGATTGAACACTTTCTACTTAGG
Sequencing primer for insertion	CptFseq	GCATAACTTAATTCTTAGAAATAACGTG

Table S3. Grading scales and histopathological analyses for the rabbit model of native valve infective endocarditis.

Heart		
Histological scoring of myocardial inflammation		
Also noted: Vegetation: present (+/-) Myocardial mineralization (+/-)	0	No inflammation
	1	Rare, scattered inflammatory cells within the aortic wall and/or myocardium
	2	Multifocal bands of inflammatory cells
	3	Large, coalescing bands of inflammatory cells with necrosis
Kidney		
Gross pathology scoring		
Also noted: Color: red/hemorrhagic (+/-) white/grey/necrotic (+/-) mottled red/grey (+/-)	0	No lesions
	1	Rare, up to 4-5 small (<4mm) multifocal lesions (infarcts) on surface
	2	Numerous larger (>5mm) multifocal lesions (infarcts) on surface
	3	Locally extensive to coalescing to diffuse lesions (infarcts) on surface
Histological scoring of foci of necropurulent inflammation		
Also scored: Ischemic necrosis (infarct) (+/-) Bacterial thrombi (+/-) Intravascular bacterial colonies (+/-) Intralesional bacteria in necrotic foci (+/-)	0	No foci
	1	One foci
	2	2 – 5 foci
	3	>5 foci
Liver		
Gross pathology scoring		
Also noted: Color: white/grey/necrotic (+/-)	0	No lesions
	1	Rare focal streak-shaped lesion/s
	2	Multifocal to coalescing streak-shaped lesions
	3	Multifocal streak-shaped and extensive to diffuse
Histological scoring of lesions (+/-)		
Centrilobular (CL) vacuolation		Diffuse to multifocal areas of vacuolated CL hepatocytes
Centrilobular (CL) necrosis		Areas of necrosis in CL hepatocytes
Infarcts		Well demarcated zones of coagulation necrosis, often surrounded by necropurulent inflammation and/or hemorrhage

Table S4. RT-qPCR Primers

Target Amplicon	Primer Pair	Sequence 5'-3'
Monocyte chemoattractant protein-1	MCP-1 For MCP-1 Rev	GCA GAA GTG GGT TCA GGA TT ATT CTT GGG TTG TGG AGT GAG
C-reactive protein	CRP For CRP Rev	GTG CTG TCA CCA GAT GAG ATT A TCG CCT TGC ACT TCA TAC TT
GM-colony stimulating factor-2	CSF2 For CSF2 Rev	GTC TCC TGA ACC TGA GTA GAG A GCT CCT GGA GGT CAA ACA TT
IL-8	CXCL8 For CXCL8 Rev	TTT GCC AAG GAG TGC TAA AGA CCA CTC TCA ATC ACT CTC AGT TC
Transforming growth factor-β1	TGF-β For TGF-β Rev	CGT GGA GCT GTA CCA GAA ATA C CAC AAC TCC GGT GAC ATC AA
ADAMTS-1	ADAMTS For ADAMTS Rev	TCA CCA CAG CCC ATG AAT TAG GGA ATC CTG GTT CAC ACC ATT A
Angiogenin	ANG For ANG Rev	GGA TAA CTC CAG GTA CAC ACA C CCG TCT CCT CAT GAT GCT TT
Serpin E1	PAI1 For PAI1 Rev	TGG GTG AAG ACA CAC ACA AA CGT TGA AGT AGA GGG CAT TCA
Urokinase plasminogen activator	PLAU For PLAU Rev	CCA CAC ACT GCT TCA TTG ATT AC TTC CAC CTC AAA CTT CAT CTC C
Acidic FGF	aFGF For aGFG Rev	GGC TCA CAG ACA CCA AAT GA GGC CAA CAA ACC AAT TCT TCT C
FGF R-2	FGFR2 For FGFR2 Rev	CAG CAC TGG AGC CTC ATT AT CAG GTG GTA CGT GTG ATT GA
HB-EGF	HBEGF For HBEGF Rev	GGG AAT GGT TTA TGC CCT AGA T CGC TGG GAA CCA TCC ATA TT
VEGF-A	VEGFA For VEGFA Rev	ATC AGT TCG AGG AAA GGG AAA G AGG CTC CAG GGC ATT AGA
VEGF-C	VEGFC For VEGFC Rev	GCT ACC TCA GCA AGA CGT TAT T ATC GGC AGG AAG TGT GAT TG
Amphiregulin	AREG For AREG Rev	ATT GGA CCT CAA TGA CAC CTA C GGA AAT CTC ACT CCC TGA AGA C
IGFBP-2	IGFBP2 For IGFBP2 Rev	CCT CTG GAG CAC CTC TAC T CAG AGA CAT CTT GCA CTG TTT G
IGFBP-3	IGFBP3 For IGFBP3 Rev	CAG AGC ACA GAT ACC CAG AAC GGA CTC AGC ACA TTG AGG AA
Pentaxin-3	PTX3 For PTX3 Rev	CAT TGT TCC TGA GGG AGG AAT C AGT CTC CCA GAG AAG GCT AAT
TIMP-1	TIMP1 For TIMP1 Rev	ATG GACTCT TGC ACA TCA CTA C GGG ATG GAT AAA CAGGGA AAC A
TIMP-4	TIMP4 For TIMP4 Rev	GGT TAC CAG GCT CAG CAT TAT GGC TGA ACG ATG TCA ACA AAC
Thrombospondin-1	TSP1 For TSP1 Rev	CTG GAC TCG CTG TAG GTT ATG GCC AAA GAC AAA TCC AGC ATA G
Endoglin	ENG For ENG Rev	GCA GGT GTC AGC AAG TAT GA GAA AGA GAG GCT GTC CAT GTT
Endothelin-1	ET1 For ET1 Rev	GTT GTT CCG TAT GGA CTT GGA GGC TAG CAC ATT GGC ATC TA
Angiopoietin-2	Ang2 For Ang2 Rev	ATC AGG ACA CAC CAC GAA TG CAT CCT CAC GTC GCT GAA TAA
Beta-actin	ACTB For ACTB Rev	GGA TCA GCA AGC AGG AGT ATG AGA AAG GGT GTA ACG CAA CTA A

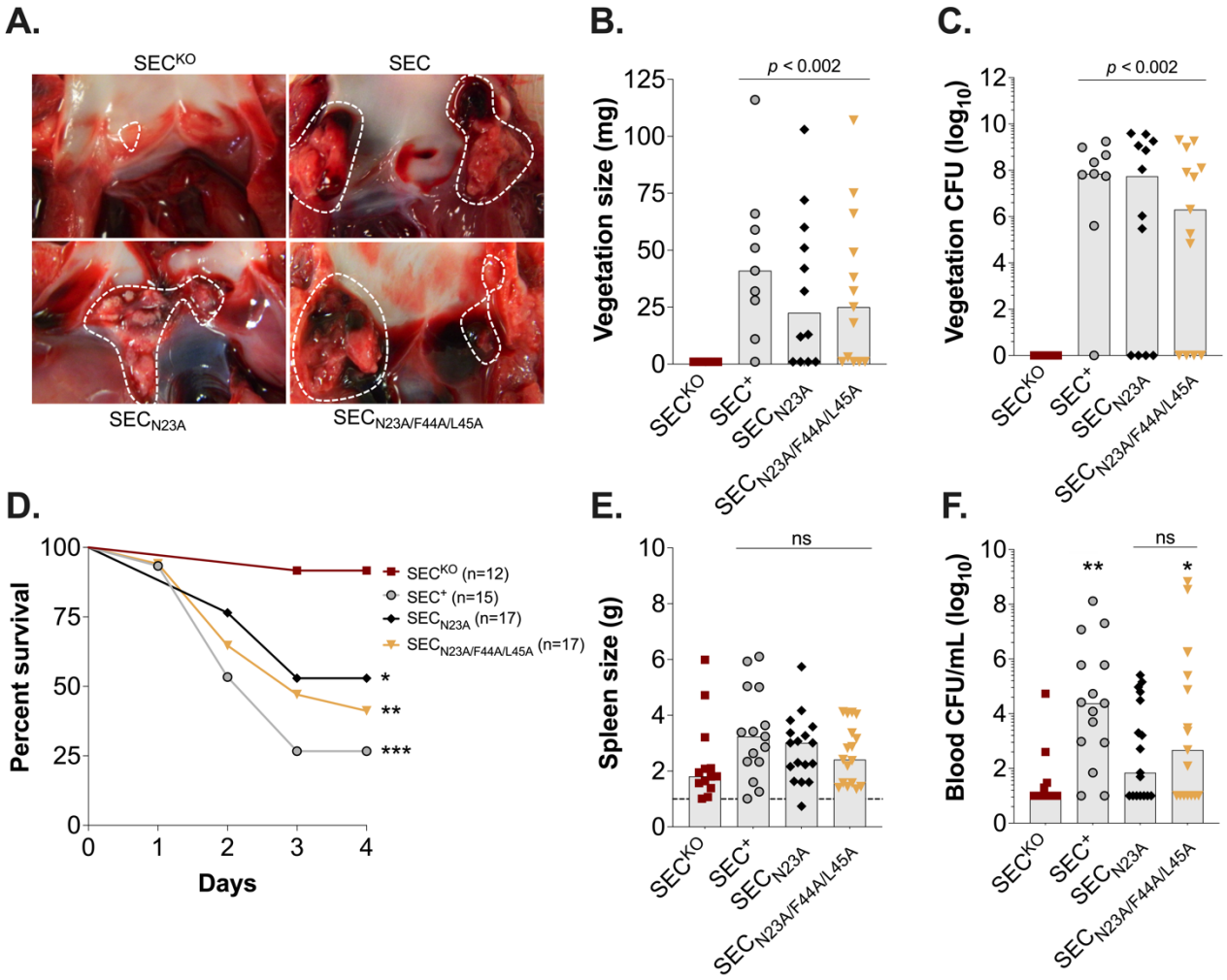

Figure 2. SEC is required for vegetation formation independent of superantigenic activity in the rabbit model of native valve infective endocarditis and sepsis. (**A**). Representative images of aortic vegetations (areas indicated with dash-lines). (**B**) Total weights of vegetations dissected from aortic valves from infected rabbits. (**C**) Bacterial counts recovered from aortic vegetations. (**A-C**) Bars represent median value. Statistical significance, one-way ANOVA with Holm-Šídák's multiple comparisons test compared to SEC^{KO}. (**D**) Percent survival of rabbits infected intravenously with $2x10^7$–$4x10^7$ CFU of indicated strain over 4 days. *, $p = 0.03$, **, $p = 0.006$, ***, $p = 0.0007$ log-rank Mantel-Cox Test. (**E**) Enlargement of the spleen resulting from *S. aureus* infection. (Dashed line) Average spleen size of uninfected rabbit controls (0.86 ± 0.1, n = 3). (**F**) Bacterial counts per milliliter of blood recovered from rabbits *post-mortem*. (**D-F**) Bars represent median value. *, $p = 0.03$, **, $p = 0.003$, ns = not significant, one-way ANOVA with Holm-Šídák's multiple comparisons test. Statistical significance compared to SEC^{KO}.

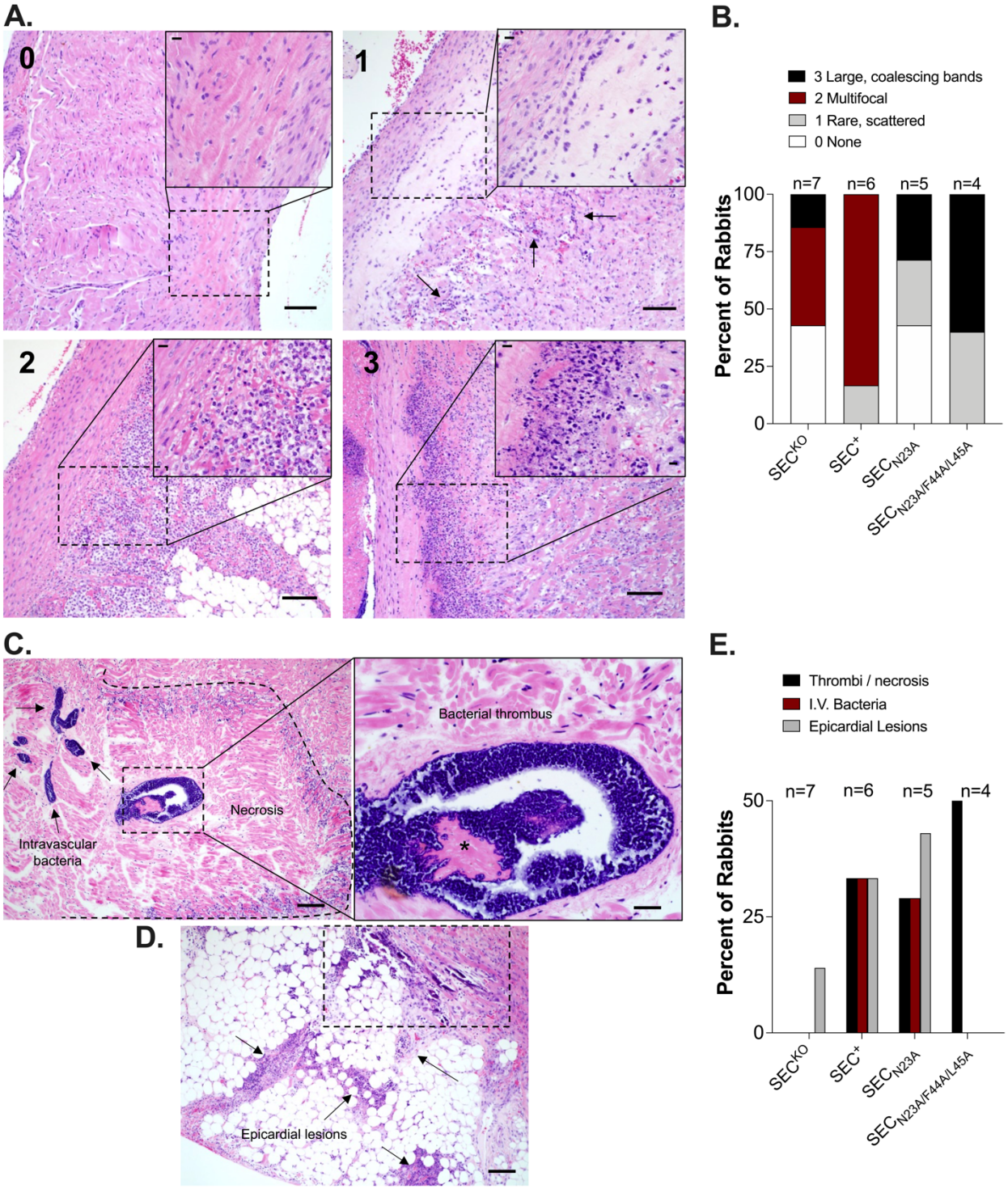
A.
0
1
2
3
B.
3 Large, coalescing bands
2 Multifocal
1 Rare, scattered
0 None
n=7
n=6
n=5
n=4
Percent of Rabbits
100
75
50
25
0
SEC^KO
SEC^+
SEC_N23A
SEC_N23A/F44A/L45A
C.
Bacterial thrombus
Necrosis
Intravascular bacteria
*
D.
Epicardial lesions
E.
Thrombi / necrosis
I.V. Bacteria
Epicardial Lesions
n=7
n=6
n=5
n=4
Percent of Rabbits
50
25
0
SEC^KO
SEC^+
SEC_N23A
SEC_N23A/F44A/L45A

Figure 3. Vegetative lesions present with bacterial infiltration, inflammation, and necrosis. (**A**) Examples of histopathologic assessment of myocardial inflammation during rabbit model of native valves infective endocarditis (Graded 0-3). Inflammation was graded based on the amount of inflammatory cell infiltrate noted within the myocardium. 0 = no inflammation, 1 = rare, scattered infiltrate (arrows), 2 = multifocal bands of infiltrate, 3 = large, coalescing bands of diffuse infiltrate with necrosis. Bar = 100 µm, inset bar = 20 µm. (**B**) Scoring of myocardial inflammation from H&E-stained images 48 – 96 h post-infection. No statistical significance among wildtype and toxoid groups, Fisher's exact test with categorical pathology grades 0-1 and grades 2-3 against SEC^{KO}. (**C**) Examples of a fibrinonecrotic focus (dotted outline; note the myocardial necrosis within the outline which is a lighter pink color), (*) a centrally located septic thrombus, and (arrows) intravascular bacteria (deeply basophilic/blue material). Left bar = 100 µm, right bar = 20 µm. (**D**) Examples of an epicardial lesion with saponification (necrosis) of epicardial fat (arrows) and a locally extensive zone of myocardial mineralization (dotted rectangle). Bar = 100 µm. (**E**) Histopathology scoring for the presence or absence of cardiac pathological findings: bacterial thrombi and associated necrosis, intravascular (IV) bacteria, and epicardial fibrin and inflammation.

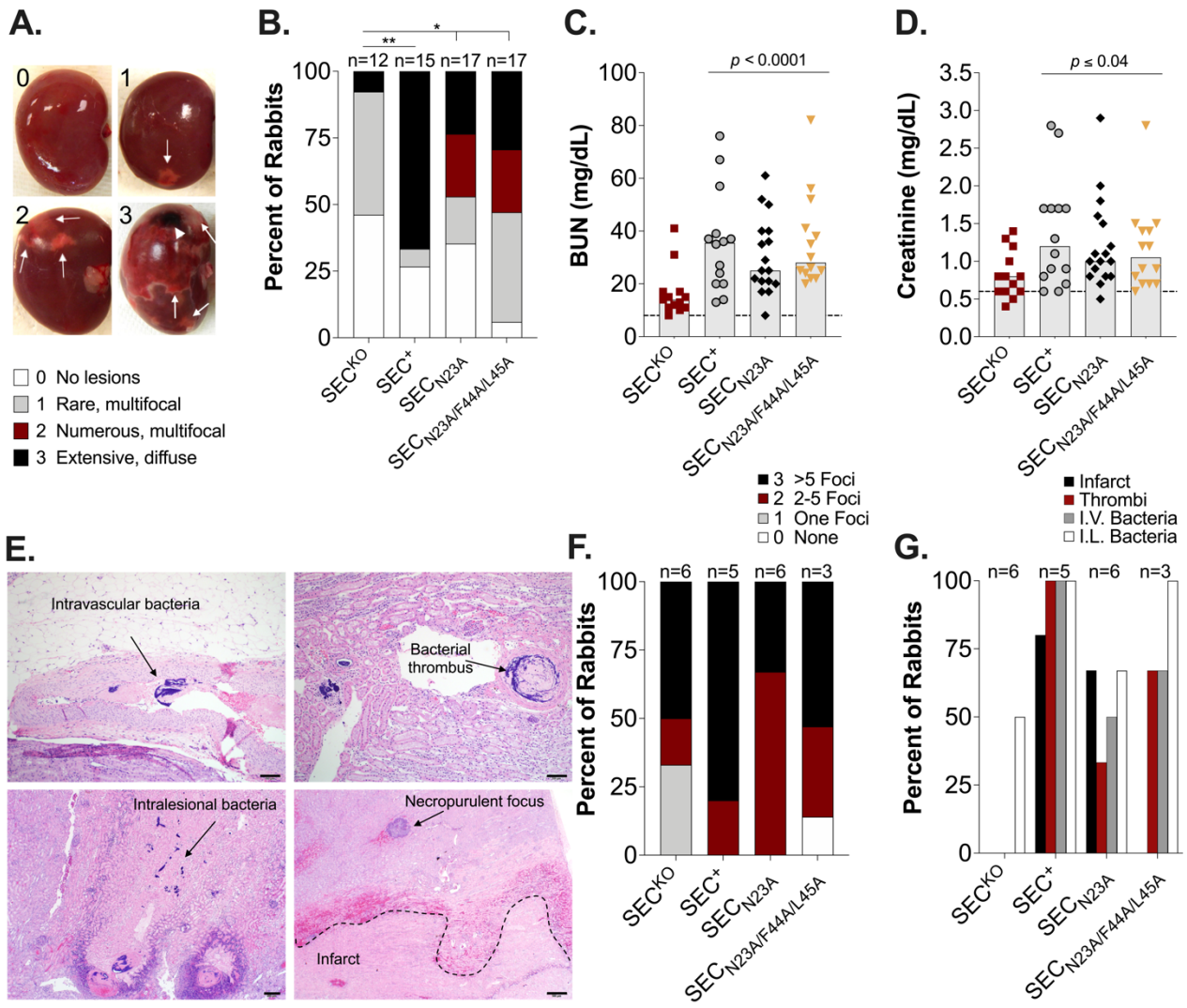

Figure 4. SEC toxoids retain the ability to cause metastatic infections and acute kidney injury. (**A**) Kidney Gross Pathology Grading Scale during rabbit model of native valves infective endocarditis (Grades 0-3). 0 = no lesions, 1 = rare, small (<4mm) multifocal lesions, 2 = numerous large (>5mm) multifocal lesions, 3 = extensive to coalescing to diffuse lesions. Arrows indicate ischemic and/or hemorrhagic lesions, arrowhead indicates a necrotic lesion. (**B**) Scoring of kidney lesions *post-mortem*. *, $p \leq 0.0432$, **, $p = 0.0047$, Fisher's exact test between categorical pathology grades 0-1 and grades 2-3 against SEC^{KO}. (**C-D**) Serum levels of analytes 48 – 96 h post-infection. Bars represent median value. Dashed line is the average analyte value of all rabbits pre-infection. All groups were tested against pre-infection analyte values and were statistically significant, $p < 0.03$, one-way ANOVA with Holm-Šídák's multiple comparisons test. (**E**) Examples of histopathologic assessment for the presence or absence of intravascular bacteria (top-left panel, arrow), bacterial thrombi (top-right panel, arrow), intralesional bacteria (bottom-left panel, arrow), and infarcts (bottom-right panel, area below dash

line). Bar = 100 µm (top-left and right panels). Bar = 200 µm (bottom-left panel). Bar = 500 µm (bottom-right panel). (**F**) Histopathologic scoring of smaller foci of necropurulent inflammation (Graded 0-3) as shown in **E**, bottom-right panel. 0 = none, 1 = one foci, 2 = 2-5 foci, 3 $\geq$ 5 foci. (**G**) Histopathologic scoring for the presence or absence of kidney lesions, as shown in **E**: Ischemic necrosis (infarct), bacterial thrombi, intravascular (I.V.) bacteria, and intralesional (I.L.) bacteria.

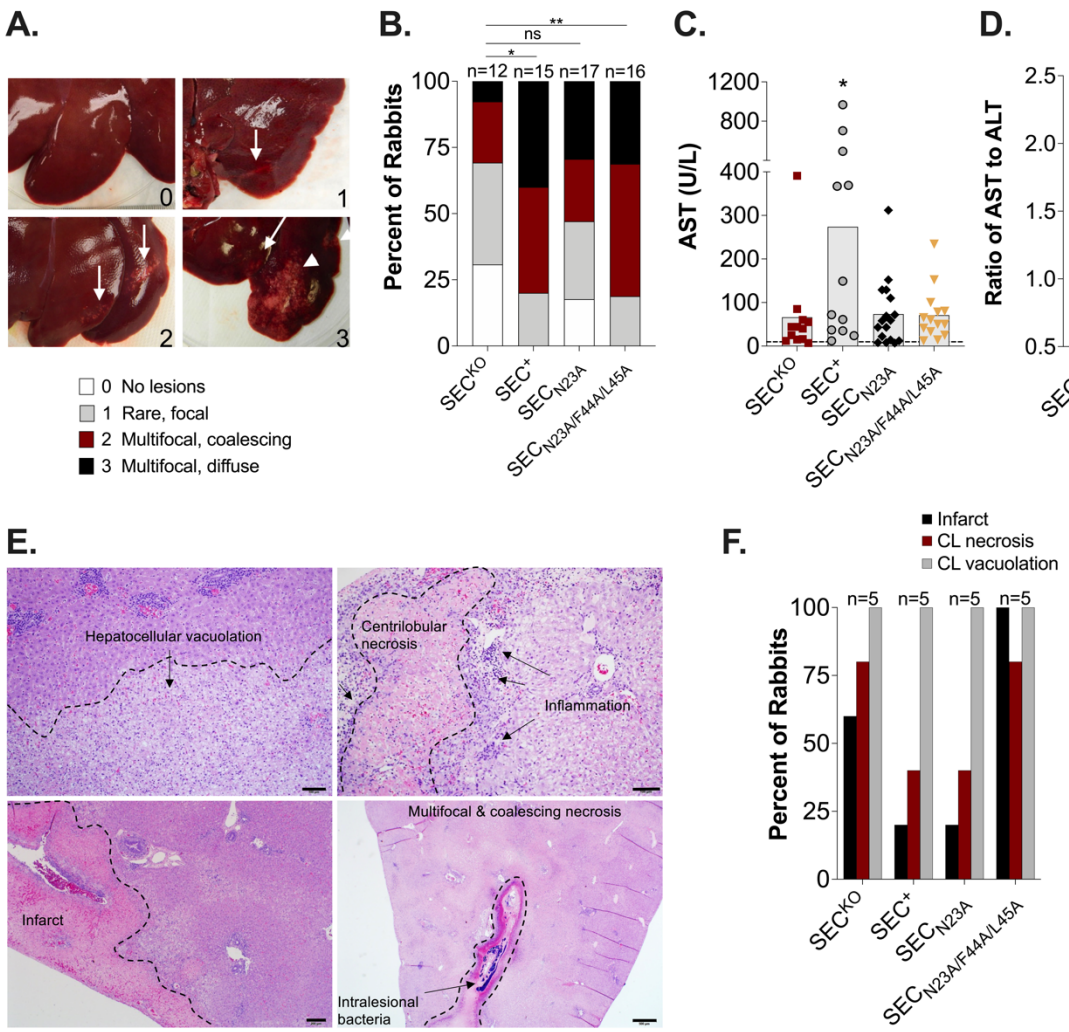

Figure 5. Superantigenicity promotes hepatocellular injury. (**A**) Liver gross pathology grading scale during rabbit model of native valves infective endocarditis (Grades 0-3). 0 = no lesions, 1 = rare, focal streak-shaped lesions, 2 = multifocal to coalescing streak-shaped lesions, 3 = multifocal streak-shaped, extensive to diffuse lesions. Arrows point to streak-shaped ischemic lesions characteristic of grade 1-3, arrowhead indicate wide-spread ischemic lesions characteristic of grade 3. (**B**) Scoring of liver pathology *post-mortem*. *, $p = 0.02$, **, $p = 0.009$, Fisher's exact test between categorical pathology grades 0-1 and grades 2-3 against SEC^{KO}. (**C-D**) Serum levels of analytes 48 – 96 h post infection. Dashed line is the average analyte or ratio value of all rabbits pre-infection. (**C**) Bars represent median value. *, $p \leq 0.01$, one-way ANOVA with the Holm-Šídák's multiple comparisons test; *S. aureus* SEC^{KO} compared to other strains. All groups were tested against pre-infection AST values and were statistically significant, $p < 0.005$. (**D**) Data are represented as mean (± SEM). *, $p \leq 0.01$, Fisher's exact test comparing ratio values 0-1.8 to values > 1.8 between *S. aureus* SEC^{+} and the rest of the experimental groups. (**E**) Examples of liver lesions observed upon histopathologic assessment. (Top-left panel) locally extensive hepatocellular vacuolation with arrow showing area under dashed line with cytoplasmic vacuolation. (Top-right panel) diffuse centrilobular necrosis (area inside dashed line), surrounded by necropurulent inflammation (arrows). (Bottom-left

panel) large zone of necrosis (infarction), area left of the dash line, with multifocal to coalescing portal hepatocellular vacuolation shown on region right of the dash line (arrows show examples). Bar = 100 µm (top-left and right panels). Bar = 200 µm (bottom-left panel). Bar = 500 µm (bottom-right panel). (**F**) Histopathologic scoring for the presence or absence infarcts, centrilobular (CL) necrosis, and centrilobular (CL) vacuolation.

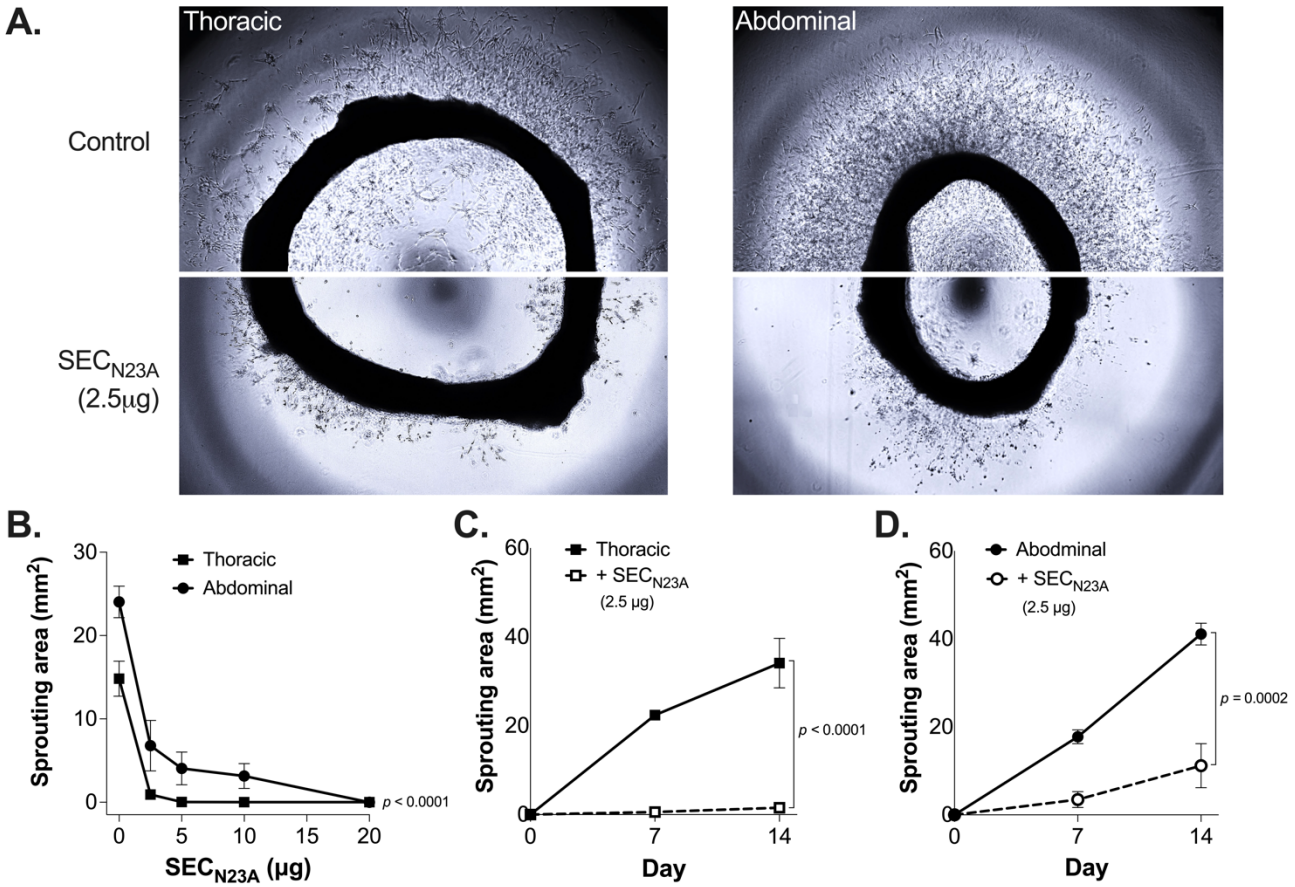

Figure 6. SEC suppresses sprouting of new capillaries in the *ex vivo* rabbit aortic ring model of angiogenesis. Thoracic and abdominal aortic ring explants were cultured in the presence of SEC_{N23A} for 14 days. (**A**) Aortic rings imaged at day 14 showing capillary network formation sprouting from the rings in culture conditions (top panels) versus treatment with 2.5 µg of SEC_{N23A} (bottom panels). (**B**) Quantification of sprouting area (mm^2) in aortic rings treated with 2.5, 5, 10, 15, and 20 µg of SEC_{N23A} for 14 days. (**C**) Time course analysis of thoracic aortic ring sprouting in the presence (solid squares) or absence (empty squares) of 2.5 µg of SEC_{N23A}. (**D**) Time course analysis of abdominal aortic ring sprouting in the presence (solid circles) or absence (empty circles) of 2.5 µg of SEC_{N23A}. (**B-D**) Statistical significance was determined by two-way ANOVA with the Holm-Šídák's multiple comparisons test. P values denote significance between treatment and no-treatment conditions.

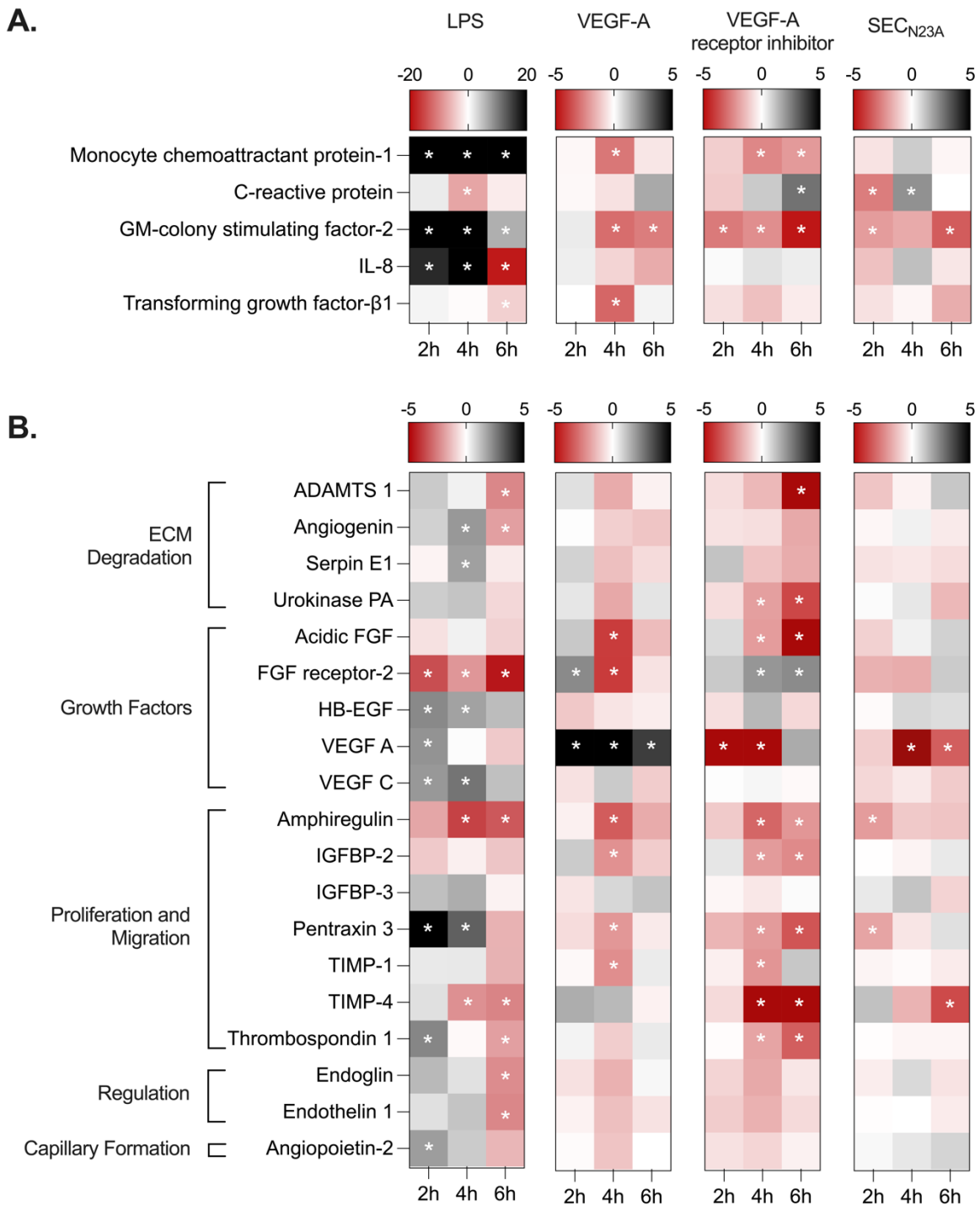

Figure 7. SEC inhibits VEGF-A expression in immortalized human aortic endothelial cells. Expression analysis of 24 angiogenesis-related genes by RT-qPCR in iHAECs treated with lipopolysaccharide (LPS, 25 ng mL^{-1}), VEGF-A (20 nM), VEGF-A receptor inhibitor (axitinib, 25 nM), or SEC_{N23A} (20 µg mL^{-1}) for 2, 4, and 6 h. (**A**) Gene products that play significant roles in inflammatory responses. (**B**) Gene products that contribute to various angiogenesis processes. *, denotes genes with 2-fold increases or decreases compared to untreated controls.